Noname manuscript No.
(will be inserted by the editor)

Adaptive Generalised Fractional Spectrogram and Its Applications

Peeyush Sahay · B. S. Teza · Pranav Kulkarni · P. Radhakrishna · Vikram M. Gadre

Received: date / Accepted: date

Abstract The generalised time-frequency transform (GTFT) is a powerful tool to analyse a large variety of frequency modulated signals. However, it is not adequate to represent the variation of frequency over time for non-stationary signals. To solve this problem, short-time GTFT and short-time GTFT based adaptive generalised fractional spectrogram (AGFS) are proposed. The AGFS is capable of providing a high concentration, high resolution, cross-term free time-frequency distribution for analysing multicomponent frequency modulated signals. It is also a generalisation of the short-time Fourier transform based spectrogram and the short-time fractional Fourier transform based spectrogram. The uncertainty principle for short-time GTFT is derived, and its time-bandwidth product is compared with other time-frequency distributions. With the help of simulated data examples, the effectiveness of AGFS is demonstrated in comparison to other time-frequency distributions for resolving and extracting individual components of multicomponent quadratic chirps. Robustness of AGFS is demonstrated under different input signal to noise ratio conditions. A local spectrogram optimisation technique is adopted for AGFS to represent simulated and real chirp signals. Finally, an application of the AGFS is presented to resolve multiple

Peeyush Sahay(✉) · B. S. Teza · Pranav Kulkarni · Vikram M. Gadre
Department of Electrical Engineering, Indian Institute of Technology, Bombay, Mumbai, India.

Peeyush Sahay
E-mail: sahay.peeyush@gmail.com

B. S. Teza
E-mail: teza.bhamidi@gmail.com

Pranav Kulkarni
E-mail: pranav.dk212@gmail.com

Vikram M. Gadre
E-mail: vmgadre@ee.iitb.ac.in

P. Radhakrishna
Electronic and Radar Development Establishment, DRDO, Bangalore, India.
E-mail: prk@lrde.drdo.in

ground moving targets in synthetic aperture radar data and obtain its focused synthetic aperture radar image.

Keywords Higher order chirps · synthetic aperture radar · short-time fractional Fourier transform · short-time generalised time-frequency transform · time-frequency distribution

1 Introduction

Non-stationary signals such as higher order polynomial chirps are present in many practical systems like radar, sonar and bio-medical signal processing [5, 7, 18, 28, 31, 42]. Non-stationary signals can be analysed using time-frequency analysis for classification, detection and feature extraction purpose in many fields [8, 9, 38]. The short-time Fourier transform (STFT) based spectrogram is one of the simplest ways of representing them in the time-frequency plane, but it is not suitable to localise a large variety of signals such as chirp signals. Therefore, alternative time-frequency distributions (TFDs) are proposed in the literature, such as the Wigner-Ville distribution (WVD) [42], polynomial WVD [7, 42], chirplet transform based spectrogram [42], polynomial chirplet transform based spectrogram [55, 56], adaptive fractional spectrogram [4, 22], S-method based spectrogram [48], STFT adaptive window based spectrogram [26], high resolution time-frequency rate representation [59], the cubic-phase function based distribution [17] and synchrosqueezing transform [2]. The WVD, the polynomial WVD, the high-resolution time-frequency rate representation, and cubic-phase function based distribution are all non-linear in nature and produce cross-terms when analysing multicomponent chirp signals. Similarly, a chirplet based spectrogram, adaptive fractional spectrogram, and STFT adaptive window based spectrogram are linear transforms but are unable to localise quadratic and higher order chirps. Similarly, synchrosqueezed STFT and synchrosqueezed wavelet transform do not provide better time-frequency resolution and parameter estimation than STFT and wavelet transform; it only improves the readability of time-frequency distribution (TFD) [21]. Hence, there is a strong requirement to represent multicomponent higher order polynomial chirps on a high concentration, high resolution cross-term free spectrogram.

As a previous research works, the generalised time-frequency transform and generalised fractional matched filtering have been shown to analyse higher order polynomial chirp signals [33, 35, 36, 37]. Recently, GTFT based generalised fractional ambiguity function (GFAF) is proposed to estimate the parameter of higher order chirp signals and to analyse higher order radar waveforms, but GFAF is non-linear transform and produces cross-terms during multicomponent signal analysis [34]. In this paper, the short-time GTFT (STGTFT) based adaptive generalised fractional spectrogram (AGFS) is proposed to analyse a large variety of multicomponent higher order polynomial and frequency modulated signals. The optimum window length of AGFS changes with signal length, hence it is adaptive in nature.

Similar to the fractional Fourier transform (FrFT), STGTFT follows the property of index additivity of angle; hence, AGFS is also computationally efficient. Non-parametric transforms such as FT, WVD, FrFT are unable to provide high concentra-

tion, high resolution TFDs for a variety of signals. AGFS overcomes this shortcoming and can provide a high concentration, high resolution TFD at its matched angle, and optimum window. AGFS is capable of providing cross-term free TFD for multicomponent signal if the components have non-overlapping STGTFTs. AGFS can analyse a variety of signals by appropriate selection of the parametric function in the GTFT kernel. The short-time nature of AGFS allows it to represent and analyse the signals with changing parameters over the signal duration. Locally optimised AGFS can represent closely spaced long and short overlapping multicomponent frequency modulated signals. These properties make AGFS superior to other TFDs.

This paper is organised as follows:

- Section 2 reviews the basics of the FrFT, GTFT and inverse GTFT.
- Section 3 presents the STGTFT, inverse STGTFT, and AGFS along with its properties and computational complexity. Mathematical derivations of some key properties are deferred to the electronic supplementary material.
- Section 4 presents the derivation and simulation results for optimum window length in time and minimum variance in GTFT domain for the quadratic chirp signal, for different cases. The compactness of the quadratic chirp in the time-frequency plane at its matched angle and optimum window variance is demonstrated.
- Section 5 presents the derivation of the uncertainty principle for the STGTFT. Subsequently, as an example, the time-bandwidth product (TBP) of quadratic chirp analysed using the cubic kernel STGTFT (ck-STGTFT), fractional Fourier based ambiguity function (FrAF) and fractional Fourier based Wigner-Ville distribution(FrWVD) are derived. TBP of quadratic chirp obtained by ck-STGTFT is shown to be lower than the TBP obtained by short-time fractional Fourier transform (STFrFT), FrAF, and STFT.
- Section 6 presents the comparison of AGFS at its optimum order and optimum window length against well-known spectrograms for representation of multicomponent quadratic chirp on the time-frequency plane.
- Section 7 presents extraction of two closely spaced multicomponent quadratic chirps using AGFS for different cases in the presence of noise and results are compared with STFT based spectrogram.
- Section 8 shows the robustness of AGFS in terms of signal to noise ratio (SNR) gain and mean error in parameter estimation under different SNR conditions. Mathematical derivation and simulation results of multicomponent quadratic chirps for SNR gain analysis of AGFS and its comparison with STFT, GTFT, FrAF, and time domain matched filtering SNR gain are also presented. Monte Carlo simulation results of mean error for estimation of quadratic frequency rate, chirp rate, and Doppler frequency parameters for multicomponent quadratic chirps using AGFS are presented, and it is compared with GTFT and FrAF based parameter estimation techniques.
- Section 9 presents a detailed description of locally optimised AGFS (LO-AGFS) method to analyse closely spaced long and short overlapping chirps. Furthermore, this section also shows a comparison of locally optimised ck-AGFS (LO-ck-AGFS)

with locally optimised STFrFT based spectrogram for the representation of closely spaced long and short overlapping quadratic chirps in the time-frequency plane.
– Section 10 presents LO-ck-AGFS of real multicomponent bat echolocation signal and its comparison against well-known TFDs.
– Section 11 presents an application of AGFS to resolve two closely spaced synthetic aperture radar (SAR) ground moving targets. It compares the distinguishing capability of AGFS with STFT based spectrogram for representation of two closely spaced SAR ground moving targets. A focused image of SAR ground moving targets after parameter estimation is presented.

2 Preliminaries

2.1 Fractional Fourier Transform

The fractional Fourier transform (FrFT) is a generalisation of the Fourier transform (FT). It depends on the parameter α, which can be interpreted as an angle of rotation in the time-frequency (TF) plane [1, 11, 25, 33, 34, 39, 46, 50]. The FrFT of a signal $x(t)$ is defined as

$$X_\alpha(f) = \int_{-\infty}^{+\infty} x(t) \cdot K_\alpha(t, f)\mathrm{d}t, \tag{1}$$

where the kernel $K_\alpha(t, f)$ of FrFT is given by [19, 34]

$$K_\alpha(t, f) = \begin{cases} (\sqrt{1 - i\cot\alpha}) \cdot \exp\Big(i\pi t_0^2 f^2 \cot\alpha + i\pi f_0^2 t^2 \cot\alpha \\ \qquad\qquad - i2\pi f t \operatorname{cosec}\alpha\Big), & \text{if } \alpha \text{ is not a multiple of } \pi \\ \delta(f_0 t - t_0 f), & \text{if } \alpha \text{ is a multiple of } 2\pi \\ \delta(f_0 t + t_0 f), & \text{if } \alpha + \pi \text{ is a multiple of } 2\pi \end{cases}$$

where t_0, f_0 are dimensional normalisation factors, $t_0^2 = \frac{T_{\max}}{f_s}$, $f_0^2 = \frac{f_s}{T_{\max}}$, $t_0^2 f_0^2 = 1$, $T_{\max}$ is the window length during FrFT and f_s is the sampling frequency. The unit of t_0 is second and f_0 is Hz.

It should be noted that at $\alpha = \frac{\pi}{2}$, K_α becomes the kernel of the Fourier transform, and hence the FrFT of the signal becomes the Fourier transform of the signal. The FrFT is a linear transform, so it does not produce cross-terms during multicomponent signal analysis.

2.2 Generalised Time-Frequency Transform

If a signal $x(t)$ has finite absolute integral (finite L^1 norm), its GTFT evaluated at parameters (α, λ) is given by

$$X_{\alpha,\lambda}(f) = \int_{-\infty}^{+\infty} x(t) \cdot K_{\alpha,\lambda}(t, f)\mathrm{d}t, \tag{2}$$

where $K_{\alpha,\lambda}(t,f)$ is the kernel of GTFT and it is defined as [33, 34, 35, 36, 37]

$$K_{\alpha,\lambda}(t,f)=\begin{cases}\sqrt{1-i\cot\alpha}\cdot\exp\Big(i\pi t_0^2 f^2\cot\alpha+i\pi f_0^2 t^2\cot\alpha & \\ -i2\pi f t\,\mathrm{cosec}\alpha+i\cdot h(\lambda,t_0 f)-i\cdot h(\lambda,f_0 t)\Big), & \text{if } \alpha \text{ is not a multiple of } \pi\\ \delta(f_0 t-t_0 f), & \text{if } \alpha \text{ is a multiple of } 2\pi\\ \delta(f_0 t+t_0 f), & \text{if } \alpha+\pi \text{ is a multiple of } 2\pi\end{cases}$$

where $h(\cdot)$ is a real valued dimensionless function, and α and λ are the real valued GTFT parameters.

One speciality of the GTFT kernel is that it follows the property of index additivity of angle [34, 37], i.e

$$\int_{-\infty}^{+\infty} K_{\alpha_1,\lambda}(t,f)K_{\alpha_2,\lambda}(f,u)\mathrm{d}f=K_{(\alpha_1+\alpha_2),\lambda}(t,u). \tag{3}$$

The GTFT is a generalisation of the FrFT, and hence a further generalisation of the Fourier transform. It can be used to analyse a much wider variety of frequency modulated signals by varying $h(\cdot)$ in the GTFT kernel. For example, if $h(\cdot)$ is defined as a polynomial function, then the resultant GTFT can be used to analyse polynomial phase signals. On the other hand, if $h(\cdot)$ is defined as a sinusoidal function, then the resultant GTFT can be used to analyse sinusoidal frequency modulated signals, and so on. Some of the GTFT kernels are as shown below:

- Cubic-kernel-GTFT (ck-GTFT) may be defined by substituting the parametric function $h(\cdot)$ as $h(\lambda,z)=\pi\lambda z^3$. Ck-GTFT is a highly useful transform used to analyse quadratic chirp signals, and is explored in detail in the later parts of this paper. It is to be noted that the ck-GTFT is similar to the third order polynomial Fourier transform (PFT) [18], with the added advantage of possessing the property of index additivity of angle [33, 34].
- Sinusoidal-kernel-GTFT may be defined by substituting a multiparametric function $h(\cdot)$ as $h(A,\phi,\lambda,z)=A\sin(\pi\lambda z+\phi)$, where A, ϕ and λ are the variable parameters, which can be tuned to match the kernel with signal for estimating parameters. This can be a useful transform to analyse certain micro-Doppler effects in radar for the classification of rotating and vibrating targets [13, 14, 34].

Inverse GTFT is defined as [34, 36]

$$x(t)=\int_{-\infty}^{\infty} X_{\alpha,\lambda}(f)\cdot K^*_{\alpha,\lambda}(t,f)\mathrm{d}f, \tag{4}$$

where $K^*_{\alpha,\lambda}(t,f)$ is the complex conjugate of $K_{\alpha,\lambda}(t,f)$. If $X_{\alpha,\lambda}(f)$ has a finite absolute sum (finite L^1 norm), the above inverse exists. GTFT is a linear transform. It does not produce cross-terms, which is beneficial during multicomponent signal analysis.

2.3 Useful Formulae

2.3.1 Gaussian Integral

$$\int_{-\infty}^{+\infty} \mathrm{e}^{-At^2 \pm 2Bt + C} \mathrm{d}t = \sqrt{\frac{\pi}{A}} \mathrm{e}^{\frac{B^2}{A} + C}, \tag{5}$$

where A, B, $C \in \mathbb{C}$, $A \neq 0$, and $Re(A) \geq 0$ [46].

2.3.2 Principle of Stationary Phase

The principle of stationary phase (PSP) is used to obtain an approximate closed-form expression for the integral of a function, whose amplitude $A(t)$ varies very slowly in comparison to the phase $\phi(t)$. Over the interval where the phase varies rapidly compared to amplitude, the contribution to the integral is negligible because positive and negative parts of the phase cancel each other. Hence, the non-zero contribution comes mainly from the stationary phase point 't_0' [34, 42] which implies

$$\int_{-\infty}^{+\infty} A(t) \cdot \mathrm{e}^{i\phi(t)} \cdot \mathrm{d}t \approx \sqrt{\frac{2\pi}{\phi''(t_0)}} \cdot A(t_0) \mathrm{e}^{i\phi(t_0)} \cdot \mathrm{e}^{\frac{i\pi}{4}}, \tag{6}$$

where $\phi''(t)$ is second derivative of the phase function $\phi(t)$ and 't_0' is the point where derivative of the phase function becomes equal to 0 ($\phi'(t_0) = 0$). At this point phase of the signal $\phi(t)$ is considered to be 'stationary'. If t_0, $t_1 \ldots t_n$ are the solutions of $\phi'(t) = 0$, then the integral can be approximated as

$$\int_{-\infty}^{+\infty} A(t) \cdot \mathrm{e}^{i\phi(t)} \cdot \mathrm{d}t \approx \sum_{k=0}^{n} \sqrt{\frac{2\pi}{\phi''(t_k)}} \cdot A(t_k) \mathrm{e}^{i\phi(t_k)} \cdot \mathrm{e}^{\frac{i\pi}{4}}. \tag{7}$$

This stationary phase approximation is accurate for high time-bandwidth products [16, 34]. If a_0 is the coefficient of t in the phase function $\phi(t)$, then PSP is valid for $|a_0| >> 0$.

3 Proposed STGTFT and AGFS

3.1 Proposed Short-Time GTFT

The short-time GTFT (STGTFT) of a signal $x(t)$ evaluated using a window $g(t)$, at parameters (α, λ), can be defined as

$$X^{g}_{\alpha,\lambda}(t, f) = \int_{-\infty}^{+\infty} x(\tau) \cdot g(\tau - t) \cdot K_{\alpha,\lambda}(\tau, f) \mathrm{d}\tau, \tag{8}$$

where $g(\cdot)$ is a window (typically Gaussian) and $K_{\alpha,\lambda}(\tau, f)$ is the GTFT kernel.

3.2 Property of Index Additivity of Angle for STGTFT :

The STGTFT follows the property of index additivity of angle as depicted by Eq. (9). It is to be noted that the ck-GTFT kernel based STGTFT is similar to the third order localised polynomial Fourier transform (LPFT), with the added advantage of possessing the property of index additivity of angle. As a result, many different STGTFTs can be calculated easily using a single STGTFT; hence STGTFT is computationally efficient.

$$X^{g}_{\alpha_1+\alpha_2,\lambda}(t,u) = \int_{-\infty}^{+\infty} X^{g}_{\alpha_1,\lambda}(t,f) K_{\alpha_2,\lambda}(f,u) \mathrm{d}f. \tag{9}$$

3.3 Proposed Inverse Short-Time GTFT

For a unit L^2 norm window $g(t)$, the inverse short-time GTFT of $X^{g}_{\alpha,\lambda}(t,f)$ having a finite L^1 norm is defined as

$$x(\tau) = \iint_{-\infty}^{+\infty} X^{g}_{\alpha,\lambda}(t,f) g^{*}(\tau - t) K^{*}_{\alpha,\lambda}(\tau,f) \mathrm{d}t \mathrm{d}f, \tag{10}$$

where $K^{*}_{\alpha,\lambda}(\tau,f)$ is the complex conjugate of the kernel $K_{\alpha,\lambda}(\tau,f)$. This inverse is unique.

Proof:

To prove this, we assume the retrieval formula as

$$\tilde{x}(\rho) = C \iint_{-\infty}^{+\infty} X^{g}_{\alpha,\lambda}(t,f) \hat{g}(\rho - t) K^{*}_{\alpha,\lambda}(\rho,f) \mathrm{d}t \mathrm{d}f, \tag{11}$$

where 'C' is a real constant and $\hat{g}(\cdot)$ is a window. Substituting Eq. (8) in Eq. (11), we get

$$\begin{aligned}
\tilde{x}(\rho) &= C \iiint_{-\infty}^{+\infty} x(\tau) g(\tau - t) K_{\alpha,\lambda}(\tau,f) \hat{g}(\rho - t) K^{*}_{\alpha,\lambda}(\rho,f) \mathrm{d}t \mathrm{d}f \mathrm{d}\tau, \\
&= C \iint_{-\infty}^{+\infty} x(\tau) g(\tau - t) \hat{g}(\rho - t) \left(\int_{-\infty}^{+\infty} K_{\alpha,\lambda}(\tau,f) K^{*}_{\alpha,\lambda}(\rho,f) \mathrm{d}f \right) \mathrm{d}t \mathrm{d}\tau, \\
&= C \iint_{-\infty}^{+\infty} x(\tau) g(\tau - t) \hat{g}(\rho - t) \cdot \Bigg(\exp\Big[i\pi \cot\alpha (f_0^2(\tau^2 - \rho^2)) \\
&\qquad - ih(\lambda, f_0\tau) - ih(\lambda, f_0\rho) \Big] \delta(\rho - \tau) \Bigg) \mathrm{d}t \mathrm{d}\tau.
\end{aligned} \tag{12}$$

Collapsing the integral in τ, we obtain:

$$\tilde{x}(\rho) = C \cdot x(\rho) \int_{-\infty}^{+\infty} g(\rho - t)\hat{g}(\rho - t)\mathrm{d}t = C \cdot x(\rho) \int_{-\infty}^{+\infty} g(t)\hat{g}(t)\mathrm{d}t. \tag{13}$$

To guarantee $\tilde{x}(\rho) = x(\rho)$, we require

$$\int_{-\infty}^{+\infty} g(t)\hat{g}(t)\mathrm{d}t = \frac{1}{C}. \tag{14}$$

We choose $\hat{g}(t) = g^*(t)$, i.e, the complex conjugate of $g(t)$. Hence, it is required that $g(t)$ have a finite L^2 norm for the inverse to exist. Under these conditions, inverse STGTFT is

$$\begin{aligned} x(\rho) &= C \iint_{-\infty}^{+\infty} X^g_{\alpha,\lambda}(t, f)g^*(\rho - t)K^*_{\alpha,\lambda}(\rho, f)\mathrm{d}t\mathrm{d}f, \\ &= \frac{1}{\int_{-\infty}^{+\infty} |g(t)|^2\mathrm{d}t} \iint_{-\infty}^{+\infty} X^g_{\alpha,\lambda}(t, f)g^*(\rho - t)K^*_{\alpha,\lambda}(\rho, f)\mathrm{d}t\mathrm{d}f. \end{aligned} \tag{15}$$

Hence, for a unit L^2 norm window $g(t)$, Eq. (15) becomes Eq. (10). It is also easy to see that the inverse is unique.

3.4 Proposed AGFS

AGFS, denoted by $\rho^{x,g}_{\alpha,\lambda}(t, f)$ of a signal $x(t)$, evaluated using a window $g(t)$, at parameters (α, λ) is defined as

$$\rho^{x,g}_{\alpha,\lambda}(t, f) = \left| \int_{-\infty}^{+\infty} x(\tau)g(\tau - t)K_{\alpha,\lambda}(\tau, f)\mathrm{d}\tau \right|^2 = |X^g_{\alpha,\lambda}(t, f)|^2, \tag{16}$$

where $K_{\alpha,\lambda}(\tau, f)$ is the GTFT kernel and window function $g(\cdot)$ is typically Gaussian.

AGFS can provide a high concentration, high resolution TFD for a variety of signals (polynomial, sinusoidal frequency modulated, etc.) by appropriate selection of the parametric function $h(\cdot)$ in the GTFT kernel. For example, AGFS can use polynomial phase GTFT kernel to analyse multicomponent polynomial phase signals. Cubic-kernel-AGFS (ck-AGFS) may be defined by using cubic-kernel GTFT to analyse multicomponent quadratic frequency modulated signals with changing parameters over its duration. On the other hand, AGFS can use sinusoidal-kernel GTFT to analyse multicomponent sinusoidal frequency modulated phase signals with changing parameters over its duration. Furthermore, AGFS with the appropriately selected kernel can be used to analyse hybrid sinusoidal frequency modulated-polynomial phase signals with changing parameters over its duration. Similarly, parametric function $h(\cdot)$ of GTFT kernel can be appropriately selected for analysis of other types of frequency modulated signals.

3.5 Properties of AGFS

3.5.1 Relationship with Other Spectrograms

It can be seen that, if:
1. $\alpha = 90^\circ$ and $h(\cdot) = 0$; $\rho^{x,g}_{\alpha,\lambda}(t, f)$ becomes the short-time FT based spectrogram.
2. $\alpha \neq 90^\circ$ and $h(\cdot) = 0$; $\rho^{x,g}_{\alpha,\lambda}(t, f)$ becomes the short-time FrFT based spectrogram. [5, 27, 46]
3. $\alpha \neq 90^\circ$ and $h(\cdot) \neq 0$; $\rho^{x,g}_{\alpha,\lambda}(t, f)$ becomes the short-time GTFT based spectrogram.

3.5.2 GTFT Form of AGFS

The GTFT form of AGFS is given by

$$\rho^{x,g}_{\alpha,\lambda}(t, f) = |\mathrm{cosec}\alpha| \left| \int_{-\infty}^{+\infty} X_{\alpha,\lambda}(f_1) G_{\frac{\pi}{2}}[(f - f_1)\mathrm{cosec}\alpha] K^*_{\alpha,\lambda}(t, f_1) \mathrm{d}f_1 \right|^2, \tag{17}$$

where $X_{\alpha,\lambda}(f_1)$ is the GTFT of $x(\tau)$ and $G_{\frac{\pi}{2}}[(f - f_1)\mathrm{cosec}\alpha]$ is the Fourier transform of window $g(\cdot)$ at frequency $(f - f_1)\mathrm{cosec}\alpha$ (see electronic supplementary material section 1).

3.5.3 Time Marginality

AGFS follows the property of time marginality, similar to the STFT based spectrogram. It is obtained by integrating AGFS over frequency. For an even window function $g(\cdot)$,

$$\int_{-\infty}^{+\infty} \rho^{x,g}_{\alpha,\lambda}(t, f) \mathrm{d}f = |x(t)|^2 *_t |g(t)|^2, \tag{18}$$

where $*_t$ is convolution over time variable t.

3.5.4 Frequency Marginality

AGFS follows the property of frequency marginality, similar to the STFT based spectrogram. It is obtained by integrating AGFS over time.

$$\int_{-\infty}^{+\infty} \rho^{x,g}_{\alpha,\lambda}(t, f) \mathrm{d}t = |X_{\alpha,\lambda}(f)|^2 *_f |G_{\frac{\pi}{2}}(f)|^2, \tag{19}$$

where $*_f$ is convolution over GTFT domain variable f and $G_{\frac{\pi}{2}}(f)$ is the symmetric Fourier transform of the window function $g(t)$.

3.5.5 Total Energy Property or Moyal Property

The total energy of AGFS of a signal is given by

$$\iint_{-\infty}^{+\infty} \rho_{\alpha,\lambda}^{x,g}(t,f)\mathrm{d}t\mathrm{d}f = \iint_{-\infty}^{+\infty} |x(\tau)|^2 |g(\tau-t)|^2 \mathrm{d}\tau\mathrm{d}t = E_x \cdot E_g, \tag{20}$$

where E_x is the energy of the signal, and E_g is the energy of the window.

3.5.6 Time Moments

Time moments property of AGFS can be derived using time marginal property of AGFS as shown in Eq. (18). For even window function $g(\cdot)$

$$\iint_{-\infty}^{+\infty} t^n \rho_{\alpha,\lambda}^{x,g}(t,f)\mathrm{d}f\mathrm{d}t = \int_{-\infty}^{+\infty} t^n \left[|x(t)|^2 *_t |g(t)|^2\right]\mathrm{d}t. \tag{21}$$

3.5.7 Frequency Moments

Frequency moments property of AGFS can be easily derived using frequency marginal property of AGFS as shown in Eq. (19). For the symmetric Fourier transform $G_{\frac{\pi}{2}}(f)$ of the window function $g(t)$

$$\iint_{-\infty}^{+\infty} f^n \rho_{\alpha,\lambda}^{x,g}(t,f)\mathrm{d}f\mathrm{d}t = \int_{-\infty}^{+\infty} f^n \left[|X_{\alpha,\lambda}(f)|^2 *_f |G_{\frac{\pi}{2}}(f)|^2\right]\mathrm{d}f. \tag{22}$$

3.5.8 Finite Support

If $x(t) = 0$ for all $t \notin [t_1, t_2]$, then $\rho_{\alpha,\lambda}^{x,g}(t,f)$ may not be strictly zero for all $t \notin [t_1, t_2]$. This is due to the fact that there exists $t \notin [t_1, t_2]$ such that $g(\tau - t)$ may still overlap with some portion of signal $x(t)$, making the spectrogram non-zero at t (see Eq. (16)). If a window function $g(\cdot)$ is of finite width T centred at the origin, then for all $t \notin \left[t_1 - \frac{T}{2}, t_2 + \frac{T}{2}\right]$, $\rho_{\alpha,\lambda}^{x,g}(t,f) = 0$. This is finite support in a weak sense. By similar arguments, if $X_{\alpha,\lambda}(f) = 0$ for all $f \notin [f_1, f_2]$, then $\rho_{\alpha,\lambda}^{x,g}(t,f)$ is not necessarily zero for all $f \notin [f_1, f_2]$ (see Eq. (17)). Hence AGFS does not follow the finite support property in a strict sense, similar to the STFT based spectrogram [15].

3.5.9 Linearity and Cross-term Free Condition

Let $\rho_{\alpha,\lambda}^{x_1,g}(t,f)$, $\rho_{\alpha,\lambda}^{x_2,g}(t,f)$ be AGFS of the signals $x_1(t)$ and $x_2(t)$ respectively. Then AGFS of the signal $x_1(t) + x_2(t)$ is given by

$$\rho_{\alpha,\lambda}^{x_1+x_2,g}(t,f) = \rho_{\alpha,\lambda}^{x_1,g}(t,f) + \rho_{\alpha,\lambda}^{x_2,g}(t,f) + X_{1_{\alpha,\lambda}}^{g}(t,f) \cdot X_{2_{\alpha,\lambda}}^{*g}(t,f) + X_{1_{\alpha,\lambda}}^{*g}(t,f) \cdot X_{2_{\alpha,\lambda}}^{g}(t,f), \tag{23}$$

where $X^{g}_{1_{\alpha,\lambda}}(t,f)$ and $X^{g}_{2_{\alpha,\lambda}}(t,f)$ are respective STGTFTs of $x_1(t)$ and $x_2(t)$.
The linearity property $\rho^{x_1+x_2,g}_{\alpha,\lambda}(t,f) = \rho^{x_1,g}_{\alpha,\lambda}(t,f) + \rho^{x_2,g}_{\alpha,\lambda}(t,f)$ holds iff

$$X^{g}_{1_{\alpha,\lambda}}(t,f)\cdot X^{*g}_{2_{\alpha,\lambda}}(t,f) + X^{*g}_{1_{\alpha,\lambda}}(t,f)\cdot X^{g}_{2_{\alpha,\lambda}}(t,f) = 0. \tag{24}$$

A sufficient (but not necessary) condition for this to hold is that $x_1(t)$ and $x_2(t)$ have non-overlapping STGTFTs. This condition is also equivalent for the AGFS to be a cross-term free TFD.

3.5.10 Time Domain Multiplication

If signals $x(t)$ and $y(t)$ have respective GTFTs $X_{\alpha,\lambda}(f)$ and $Y_{\alpha,\lambda}(f)$, then a signal $z(t) = x(t)y(t)$ has an AGFS given by

$$\rho^{z,g}_{\alpha,\lambda}(t,f) = \left| \int_{-\infty}^{+\infty} X_{\alpha,\lambda}(f_1) K_{\alpha,\lambda}(t,f) K^{*}_{\alpha,\lambda}(t,f_1)\cdot [G_{\frac{\pi}{2}}(f^{'}) *_{f'} Y_{\frac{\pi}{2}}(f^{'}) \mathrm{e}^{i2\pi t f^{'}}]\mathrm{d}f_1 \right|^2, \tag{25}$$

where $*_{f'}$ is convolution over variable $f^{'} = (f - f_1)\mathrm{cosec}\alpha$ and $Y_{\frac{\pi}{2}}(f^{'})$ is Fourier transform of $y(t)$ at frequency $f^{'}$ (see electronic supplementary material section 2).

3.5.11 Discretization in Time

If $z(t)$ is sampled version of $x(t)$ with sampling frequency f_s, then AGFS of $z(t)$ is periodic with period $f_s \sin\alpha$ in the GTFT domain. AGFS of $z(t)$ with window $g(t)$ is given as

$$\rho^{z,g}_{\alpha,\lambda}(t,f) = \sum_{n=-\infty}^{\infty} \rho^{x,g}_{\alpha,\lambda}(t, f - n f_s \sin\alpha), \tag{26}$$

where n takes integer values. Periodicity property of AGFS is similar to the periodicity property of FrFT [44]. This property can be proved using the time domain multiplication property of AGFS, with one of the signals being an impulse train.

In addition, the following properties mentioned in Eq. (27-31) can be proved for a cubic phase kernel AGFS (i.e. for a ck-AGFS) $h(\lambda, t_0 f) = \pi\lambda(t_0 f)^3$ and $h(\lambda, f_0 t) = \pi\lambda(f_0 t)^3$:

3.5.12 Time Scaling

If the ck-AGFS of $x(t)$ analysed using window function $g(t)$ is $\rho^{x,g}_{\alpha,\lambda}(t,f)$, then the ck-AGFS of $y(t) = \sqrt{p}\cdot x(p\cdot t)$ is given by

$$\rho^{y,g}_{\alpha,\lambda}(t,f) = |Y^{g}_{\alpha,\lambda}(t,f)|^2 = \left|\frac{\mathrm{cosec}\alpha}{p\cdot\mathrm{cosec}\beta}\right| \rho^{x,g_1}_{\beta,\gamma}\left(p\cdot t, \frac{f\cdot\mathrm{cosec}\alpha}{p\cdot\mathrm{cosec}\beta}\right), \tag{27}$$

where, $\cot\beta = \cot\alpha/p^2$, $\gamma = \lambda/p^3$ and $g_1(t) = g(t/p)$ (see electronic supplementary material section 3).

3.5.13 Time Delay

If the ck-AGFS of $x(t)$ analysed using window function $g(t)$ is $\rho^{x,g}_{\beta,\lambda}(t,f)$, then the ck-AGFS of time delayed signal $y(t) = x(t - t_d)$ is given by

$$\rho^{y,g}_{\alpha,\lambda}(t,f) = \left|\frac{\text{cosec}\alpha}{\text{cosec}\beta}\right| \rho^{x,g}_{\beta,\lambda}\left(t - t_d, \frac{\text{cosec}\alpha}{\text{cosec}\beta}\left[f + \frac{3}{2}f_0^3\lambda t_d^2 \sin\alpha - f_0^2 t_d \cos\alpha\right]\right), \quad (28)$$

where t_d is the time delay and $\cot\beta = \cot\alpha - 3f_0\lambda t_d$, (see electronic supplementary material section 4).

3.5.14 Frequency Shift

If the ck-AGFS of $x(t)$ is analysed using window function $g(t)$ is $\rho^{x,g}_{\alpha,\lambda}(t,f)$, then the ck-AGFS of frequency shifted signal $y(t) = x(t)\exp(2\pi f_d t)$ is given by

$$\rho^{y,g}_{\alpha,\lambda}(t,f) = \rho^{x,g}_{\alpha,\lambda}(t, f - f_d \sin\alpha). \quad (29)$$

where f_d is the frequency shift, (see electronic supplementary material section 5).

3.5.15 Convolution Property

Here we define the convolution operation in a different sense to preserve the frequency domain multiplication equivalence of time domain convolution [57]. Let $h(\cdot)$ be the convolution of $f(\cdot)$ and $g(\cdot)$. For the cubic phase kernel of GTFT, we define

$$h(t) = (\sqrt{1 - i\cot\alpha}) \cdot \tilde{h}(t)\mathrm{e}^{-i\pi f_0^2 t^2 \cot\alpha + i\pi f_0^3 \lambda t^3},$$

where $\tilde{h}(t) = \tilde{f}(t) * \tilde{g}(t)$ is the standard convolution with $\tilde{f}(t)$ and $\tilde{g}(t)$ defined as

$$\tilde{f}(t) = f(t)\mathrm{e}^{i\pi f_0^2 t^2 \cot\alpha - i\pi f_0^3 \lambda t^3},$$

$$\tilde{g}(t) = g(t)\mathrm{e}^{i\pi f_0^2 t^2 \cot\alpha - i\pi f_0^3 \lambda t^3}.$$

Taking the cubic phase GTFT kernel and window function to be $g_1(\cdot)$, the expression for AGFS of $h(\cdot)$ is given as $|H^{g_1}_{\alpha,\lambda}(t,f)|^2$, where

$$H^{g_1}_{\alpha,\lambda}(t,f) = [(g(t)K_{\alpha,\lambda}(t,f)) *_t F^{g_1}_{\alpha,\lambda}(t,f)] \cdot \mathrm{e}^{-i\pi t_0^3 \lambda f^3 - i\pi t_0^2 f^2 \cot\alpha}, \quad (30)$$

where $F^{g_1}_{\alpha,\lambda}(t,f)$ is the STGTFT of $f(\cdot)$ with window $g_1(\cdot)$ (see electronic supplementary material section 6).

3.5.16 Relationship with Modified STFT based Spectrogram

If $\rho^{y,g}_{\frac{\pi}{2}}(t,f)$, is a modified STFT [1] of signal $x(t)$, then the relationship of modified STFT based spectrogram with cubic phase GTFT kernel is given by (see electronic supplementary material section 8):

$$\rho^{y,g}_{\frac{\pi}{2}}(t,f) = \Bigg| C_{\lambda,\alpha,\beta}(t,f) \int_{-\infty}^{\infty} X_{\alpha,\lambda}(f_1) \cdot G^{*}_{\beta,\lambda}\big(P_{\alpha,\beta} \cdot (f_1 - u_{\alpha,\lambda})\big) K_{\gamma,\eta}(t_3, P_{\alpha,\beta} u_{\alpha,\lambda}) \mathrm{d}f_1 \Bigg|^2, \tag{31}$$

where

$$C_{\lambda,\alpha,\beta}(t,f) = \frac{(\sqrt{1 - i\cot\alpha})}{(\sqrt{1 - i\cot\beta})(\sqrt{1 - i\cot\gamma})} \exp\Bigg[i\pi \Bigg(- ft + \lambda f_0^3 t^3 - t^2 f_0^2 \cot\alpha - \lambda t_0^3 P^3_{\alpha,\beta} u^3_{\alpha,\lambda} + t_0^2 P^2_{\alpha,\beta} u^2_{\alpha,\lambda} \cot\beta - f_0^2 t_3^2 \cot\gamma + f_0^3 t_3^3 \eta \Bigg) \Bigg], \tag{32}$$

$$t_3 = \frac{1}{\mathrm{cosec}\gamma} \left[t_0^2 P_{\alpha,\beta} u_{\alpha,\lambda} \cot\beta - \frac{3}{2} \lambda t_0^3 P^2_{\alpha,\beta} u^2_{\alpha,\lambda} - \frac{t \mathrm{cosec}\alpha}{P_{\alpha,\beta}} \right], \tag{33}$$

$$\cot\gamma = \cot\beta - 3\lambda t_0 P_{\alpha,\beta} u_{\alpha,\lambda} - \frac{\cot\alpha}{P^2_{\alpha,\beta}}, \quad \eta = 1 - \frac{1}{P^3_{\alpha,\beta}}, \quad P_{\alpha,\beta} = \frac{\mathrm{cosec}\beta}{\mathrm{cosec}\alpha}, \tag{34}$$

$$\cot\beta = \cot\alpha - 3\lambda f_0 t, \quad \text{and} \quad u_{\alpha,\lambda} = f \sin\alpha + t f_0^2 \cos\alpha - \frac{3}{2} \lambda f_0^3 t^2 \sin\alpha. \tag{35}$$

If $\lambda = 0$ in Eq. (31), then we can get the relationship of the modified STFT based spectrogram with FrFT kernel. A similar result has been derived in the Almeida paper [1] for FrFT case, and it is given by:

$$\rho^{y,g}_{\frac{\pi}{2}}(t,f) = \Bigg| \exp\left(i\pi u_{\alpha,\lambda=0} \cdot v_\alpha\right) \int_{-\infty}^{\infty} X_\alpha(f_1) \cdot G^{*}_{\alpha}\big(f_1 - u_{\alpha,\lambda=0}\big) \exp(-i2\pi f_1 v_\alpha) \mathrm{d}f_1 \Bigg|^2, \tag{36}$$

where $v_\alpha = t_0^2 f \cos\alpha - t \sin\alpha$, and $u_{\alpha,\lambda=0} = f \sin\alpha + t f_0^2 \cos\alpha$. $X_\alpha(f_1)$ is FrFT of the signal $x(\tau)$, $G_\alpha(f_1 - u_{\alpha,\lambda=0})$ is FrFT of the window $g(\tau)$ at frequency $(f_1 - u_{\alpha,\lambda=0})$, and $\rho^{y,g}_{\frac{\pi}{2}}(t,f)$ is STFrFT based spectrogram of signal $x(t)$ with window $g(t)$.

As shown in Eq. (36), the FrFT kernel rotates modified STFT with an angle α [1]. Similarly, as a generalisation of FrFT, GTFT with any kernel rotates STGTFT with an angle of α at a given λ. It can be easily proved using the index additivity of angle property of GTFT kernel.

$$X^{g}_{\alpha_1+\alpha_2,\lambda}(t,u) = \int_{-\infty}^{+\infty} X^{g}_{\alpha_1,\lambda}(t,f) K_{\alpha_2,\lambda}(f,u) \mathrm{d}f. \tag{37}$$

As a generalisation of FrFT, GTFT also rotates the ambiguity function. Recently, as our previous research work, generalised fractional ambiguity function (GFAF) is proposed, which is a generalisation of the Fourier transform based ambiguity function, and the fractional Fourier transform based ambiguity function. Since GFAF also follow index additivity of angle property, hence GTFT with any kernel rotates GFAF with an angle of α at a given λ [34].

3.6 Computation Complexity of Digital AGFS

AGFS is computed from the short-time GTFT. Computational complexity of the GTFT for an N length quadratic chirp signal is $O(N \log_2 N)$. If N/ϵ is the step size during the sliding window, then the digital computational complexity of AGFS will be $O(\epsilon N \log_2 N)$. For step size 1, i.e. $\epsilon = N$, complexity is $O(N^2 \log_2 N)$ [25][46].

4 Ck-AGFS of Quadratic Chirps

Consider a quadratic chirp signal $x(\tau)$ and a unit energy Gaussian window function $g(\tau)$ as

$$x(\tau) = A \exp\left(i\pi c\tau^3 + i\pi a\tau^2 + i2\pi f_d \tau\right), \tag{38}$$

$$g(\tau) = (\pi\sigma_{t_0}^2)^{-\frac{1}{4}} \exp\left(-\frac{\tau^2}{2\sigma_{t_0}^2}\right), \tag{39}$$

where c is the quadratic rate, a is the chirp rate, f_d is the Doppler frequency, A is the amplitude and $\sigma_{t_0}^2$ is time variance of Gaussian window. The STGTFT of $x(t)$ is calculated using cubic phase GTFT kernel $h(\lambda, t_0 f) = \pi\lambda(t_0 f)^3$ and $h(\lambda, f_0 t) = \pi\lambda(f_0 t)^3$.

4.1 Analytical Expression of ck-AGFS for Unmatched Cubic Phase

The STGTFT of $x(t)$ for unmatched cubic phase is

$$\begin{aligned} X_{\alpha,\lambda}^{g}(t,f) &= \int_{-\infty}^{+\infty} x(\tau) g(t-\tau) K_{\alpha,\lambda}(\tau, f) \mathrm{d}\tau \\ &= A_0 \cdot \mathrm{e}^{i\phi_0(f)} \int_{-\infty}^{+\infty} \exp\left(-\frac{(t-\tau)^2}{2\sigma_{t_0}^2}\right) \\ &\quad \cdot \exp(i\pi c^{'}\tau^3 + i\pi a^{'}\tau^2 + i2\pi f^{'}\tau)\mathrm{d}\tau, \end{aligned} \tag{40}$$

where,

$$\begin{aligned} &A_0 = A(\pi\sigma_{t_0}^2)^{\frac{-1}{4}} \sqrt{1 - i\cot\alpha},\ \phi_0(f) = \lambda\pi t_0^3 f^3 + i\pi t_0^2 f^2 \cot\alpha, \\ &c' = c - f_0^3\lambda,\ f' = f_d - f\,\mathrm{cosec}\alpha, a' = a + f^2\cot\alpha. \end{aligned}$$

Using the stationary phase approximation Eq. (7) on the integral, the ck-AGFS of the quadratic chirp for $|f_d - f\text{cosec}\alpha| >> 0$ is obtained as

$$\begin{aligned}\left|X^g_{\alpha,\lambda}(t,f)\right|^2 \approx |B|^2\Bigg[&\exp\left(-\frac{\left(\sqrt{a'^2-6c'f'}-(a'+3c't)\right)^2}{(3c'\sigma_{t_0})^2}\right)\\&+\exp\left(-\frac{\left(\sqrt{a'^2-6c'f'}+(a'+3c't)\right)^2}{(3c'\sigma_{t_0})^2}\right)\Bigg],\end{aligned} \tag{41}$$

where

$$|B|^2 = \frac{|A|^2|\text{cosec}\alpha|}{\sqrt{\pi\sigma^2_{t_0}(a'^2-6c'f')}}.$$

For matching cubic phase, $c^{'}$ approaches zero and Eq. (41) becomes

$$\begin{aligned}\lim_{c'\to 0}\left|X^g_{\alpha,\lambda}(t,f)\right| \approx &\frac{|A|}{(\pi\sigma^2_{t_0})^{\frac{1}{4}}\cdot(a\sin\alpha+f_0^2\cos\alpha)^{\frac{1}{4}}}\\&\cdot\exp\left[-\frac{1}{2}\left(\frac{f-(f_d\sin\alpha+at\sin\alpha+f_0^2t\cos\alpha)}{\sigma_{t_0}(a\sin\alpha+f_0^2\cos\alpha)}\right)^2\right].\end{aligned} \tag{42}$$

This is the approximate STGTFT expression at unmatched cubic phase condition when $|f_d - f\text{cosec}\alpha| >> 0$. An exact expression of ck-AGFS for matched cubic phase condition is derived using the Gaussian integral formula of Eq. (5) in Section 4.2.

4.2 Expression for Optimum Window Size of Quadratic Chirp ck-AGFS for Matched Cubic Phase

We consider a quadratic chirp signal $x(\tau)$ and a unit energy Gaussian window function $g(\tau)$ as in Eq.(38) and Eq. (39). Then

$$\rho^{x,g}_{\alpha,\lambda}(t,f) = \left|\int_{+\infty}^{+\infty} x(\tau)g(\tau-t)K_{\alpha,\lambda}(\tau,f)\text{d}\tau\right|^2 = \left|X^g_{\alpha,\lambda}(t,f)\right|^2. \tag{43}$$

To get the optimum window, we concentrate on the STGTFT part

$$\begin{aligned}\left|X^g_{\alpha,\lambda}(t,f)\right| = \Bigg|&(A\sqrt{1-i\cot\alpha})(\pi\sigma^2_{t_0})^{-\frac{1}{4}}\int_{-\infty}^{+\infty}\text{e}^{i\pi c\tau^3+i\pi a\tau^2+i2\pi f_d\tau}\\&\cdot\exp\left[i\pi t_0^2f^2cot\alpha+i\pi f_0^2\tau^2cot\alpha-i2\pi f\tau\text{cosec}\alpha\right.\\&\left.-i\lambda\pi(f_0\tau)^3+i\lambda\pi(t_0f)^3\right]\exp\left(-\frac{(\tau-t)^2}{2\sigma^2_{t_0}}\right)\text{d}\tau\Bigg|.\end{aligned} \tag{44}$$

Solving this integral at matched GTFT of cubic phase condition, $f_0^3\lambda = c$ using Gaussian integral formula of Eq. (5) gives

$$\left|X^g_{\alpha,\lambda}(t,f)\right| = \frac{|A|}{(\pi\sigma_{t_0}^2)^{\frac{1}{4}}} \frac{\sqrt{\pi|\mathrm{cosec}\alpha|}}{\left[\left(\frac{1}{2\sigma_{t_0}^2}\right)^2 + \pi^2(a + f_0^2\cot\alpha)^2\right]^{\frac{1}{4}}} \cdot \exp\left[-\frac{1}{2}\frac{\left(f - (at\sin\alpha + f_d\sin\alpha + f_0^2 t\cos\alpha)\right)^2}{\frac{\sin^2\alpha}{\sigma_{t_0}^2 4\pi^2} + \sigma_{t_0}^2(f_0^2\cos\alpha + a\sin\alpha)^2}\right]. \quad (45)$$

Hence, the exact form of cubic kernel STGTFT of a quadratic chirp in Eq. (45) almost (but not exactly) matches with the approximate form of cubic kernel STGTFT of unmatched cubic phase at limiting condition as shown in Eq. (42).

This is a Gaussian expression in f, and its variance can be extracted by comparison with the standard Gaussian form as

$$\sigma_{\alpha_0}^2 = \frac{\sin^2\alpha}{\sigma_{t_0}^2 4\pi^2} + \sigma_{t_0}^2(f_0^2\cos\alpha + a\sin\alpha)^2. \quad (46)$$

Here, $\sigma_{t_0}^2$ is the variance of the Gaussian window in time and its unit is sec^2. $\sigma_{\alpha_0}^2$ is the variance of the Gaussian window in GTFT domain, and its unit is Hz^2. Variance should be dimensionless in the GTFT domain, so dimension normalisation of $\sigma_{\alpha_0}^2$ is required, and it is done as shown below:

$$\sigma_{t_0}^2 = \frac{\sigma_t^2}{f_s^2},$$

where σ_t^2 is the variance in time domain in terms of samples (dimensionless).

$$\therefore \sigma_{\alpha_0}^2 = \frac{f_s^2\sin^2\alpha}{\sigma_t^2 4\pi^2} + \frac{\sigma_t^2}{f_s^2}(f_0^2\cos\alpha + a\sin\alpha)^2. \quad (47)$$

Similarly, if σ_α^2 is the variance of Gaussian window in GTFT domain, then

$$\therefore \sigma_\alpha^2 = f_s^2\sigma_{\alpha_0}^2 = \frac{f_s^4\sin^2\alpha}{\sigma_t^2 4\pi^2} + \sigma_t^2(f_0^2\cos\alpha + a\sin\alpha)^2. \quad (48)$$

σ_α^2 has the unit Hz^4 in the GTFT domain. Hence, dimension normalisation in the GTFT domain is required. It is done by defining

$$\sigma_{\alpha'}^2 = t_0^4\sigma_\alpha^2 = \frac{t_0^4 f_s^4\sin^2\alpha}{\sigma_t^2 4\pi^2} + \sigma_t^2(\cos\alpha + t_0^2 a\sin\alpha)^2, \quad (49)$$

where $\sigma^2_{\alpha'}$ is the variance in the GTFT domain in terms of samples (dimensionless). Considering $N = f_s\tau$ and half-length sliding window of STGTFT ($T_{\max} = \frac{\tau}{2}$), with τ as the signal duration leads to $t_0^2 = \frac{\tau}{2f_s}$.

$$\therefore \sigma^2_{\alpha'} = \left(\frac{N}{4\pi}\right)^2 \frac{\sin^2\alpha}{\sigma_t^2} + \sigma_t^2\left(\cos\alpha + \frac{a\tau}{2f_s}\sin\alpha\right)^2. \tag{50}$$

Hence, for a quadratic chirp signal, it can be observed that:

1. If cubic kernel STGTFT (ck-STGTFT) is 'cubic matched', then the cubic portion of the phase function of the signal will be cancelled using the ck-GTFT kernel. If cubic kernel STGTFT (ck-STGTFT) is 'matched ck-STGTFT', then the cubic *and* quadratic portions of the phase functions of the signal will be canceled using the ck-GTFT kernel.
2. Any Gaussian window function in the time domain has a Gaussian cubic-matched ck-STGTFT response.
3. Shift parameter t, quadratic rate c, and Doppler frequency f_d do not affect the variance of the Gaussian window in the cubic-matched ck-STGTFT domain.

4.3 Optimum Time Window for Minimum Variance in Cubic-Matched ck-STGTFT Domain

For an optimum σ_t^2, which gives a minimum $\sigma^2_{\alpha'}$,

$$\frac{\mathrm{d}\sigma^2_{\alpha'}}{\mathrm{d}\sigma_t^2} = -\left(\frac{N}{4\pi}\right)^2 \frac{\sin^2\alpha}{\sigma_t^4} + \left(\cos\alpha + \frac{a\tau}{2f_s}\sin\alpha\right)^2 = 0, \tag{51}$$

$$\sigma^2_{t_{\text{opt}}} = \left|\frac{\frac{N}{4\pi}\sin\alpha}{\cos\alpha + \frac{a\tau\sin\alpha}{2f_s}}\right|. \tag{52}$$

The minimum $\sigma^2_{\alpha'}$ at $\sigma^2_{t_{\text{opt}}}$ is given by

$$\sigma^2_{\alpha'_{\min}} = \left|\frac{N}{2\pi}\sin\alpha\left(\cos\alpha + \frac{a\tau\sin\alpha}{2f_s}\right)\right|. \tag{53}$$

Consider the following cases:

1. When $a = 0$ and $\alpha \neq \alpha_{\text{opt}}$, from Eq. (52) and Eq. (53)

$$\sigma^2_{t_{\text{opt}}} = \left|\frac{N}{4\pi}\tan\alpha\right|, \tag{54}$$

$$\sigma^2_{\alpha'_{\min}} = \left|\frac{N}{4\pi}\sin 2\alpha\right|. \tag{55}$$

A similar result was obtained in [10] for a Gaussian window in FrFT domain.

2. When $a \neq 0$ and $\alpha = 90^\circ \neq \alpha_{\text{opt}}$ (STFT case), from Eq. (52) and Eq. (53)

$$\sigma^2_{t_{\text{opt}}}\Big|_{\alpha=90^\circ} = \left|\frac{f_s^2}{2\pi a}\right|, \tag{56}$$

$$\sigma^2_{\alpha'}\Big|_{\alpha=90^\circ} = \left|\frac{a\tau^2}{4\pi}\right|. \tag{57}$$

   A similar result was obtained in [26][15] for Gaussian window in STFT domain.
3. When $a \neq 0$ and $\alpha \neq \alpha_{\text{opt}}$, $\sigma^2_{t_{\text{opt}}}$ and $\sigma^2_{\alpha'}$ are given by the generic formulae Eq. (52) and Eq. (53) respectively.
4. When $a\epsilon(-\infty, \infty)$ and $\alpha = \alpha_{\text{opt}}$, where α_{opt} is optimum matched angle, Eq. (53) becomes

$$\sigma^2_{\alpha'_{\text{min}}} = \left(\frac{N}{4\pi}\right)^2 \frac{\sin^2\alpha}{\sigma^2_{t_{\text{opt}}}}. \tag{58}$$

   This means that a minimum variance in the GTFT domain is obtained at infinite time windowing. It is similar to the uncertainty principle, which is derived in subsequent section 5. Infinite time windowing is not practical, and a compromise is needed. Hence $5\sigma_t$ window can be considered, which contains 98.75% energy in $\frac{N}{2}$ (assuming half signal length Gaussian window).

$$\therefore 5\sigma_{t_{\text{opt}}} = \frac{N}{2}, \implies \sigma_{t_{\text{opt}}} = \frac{N}{10} \quad \text{for 98.75\% energy.} \tag{59}$$

$$\therefore (\sigma_{\alpha'})_{\text{min}} = \left[\left(\frac{N}{4\pi}\right)^2 \frac{\sin^2(\alpha)}{\left(\frac{N}{10}\right)^2}\right]^{\frac{1}{2}} = \frac{10}{4\pi}\sin\alpha. \tag{60}$$

   This $(\sigma_{\alpha'})_{\text{min}}$ is always less than unity. Hence, Case 4 ($f_0^3\lambda = c$ and $\alpha = \alpha_{\text{opt}}$) gives the least standard deviation in GTFT domain out of all cases.

4.4 Results

4.4.1 Optimum Time Window and Minimum Variance in Cubic Matched ck-STGTFT Domain for Different Cases of Single Component Quadratic Chirp

The simulation results are listed in Table 1 for different cases of Gaussian window based cubic-matched ck-STGTFT domain analysis of single component quadratic chirps. Table 1 is constructed using the following procedure:

1. Mean $(\sigma_{\alpha'})_{\text{min}}$ is the average standard deviation of the Gaussian response in GTFT domain across different window positions. Variance in GTFT domain is calculated based on the three sigma rule of the Gaussian for each window position, meaning that 99.7% energy of the Gaussian distribution lies within first three standard deviations on each side of the mean.
2. Mean $\sigma_{t_{\text{opt}}}$ is optimum time window length, which gives least mean $(\sigma_{\alpha'})_{\text{min}}$.

3. Estimated optimum standard deviation in time domain ($Est.\ \sigma_{t_{\text{opt}}}$) and estimated optimum standard deviation in cubic-matched ck-STGTFT domain ($Est.(\sigma_{\alpha'})_{\min}$) are calculated based on the formula derived for $\sigma_{t_{\text{opt}}}$ and $(\sigma_{\alpha'})_{\min}$ for different cases in subsection 4.3.
4. Energy concentration measure (ECM) [7, pp. 401-408] is used as a measure for comparing the best TFD concentration.

$$M = \frac{\left(\sum_t \sum_f \left|(\rho^{x,g}_{\alpha,\lambda}(t,f))\right|^{\frac{1}{2}}\right)^2}{\sum_t \sum_f \left|\rho^{x,g}_{\alpha,\lambda}(t,f)\right|}. \tag{61}$$

   ECM is a standard criterion for measuring concentration for any type of window function. The window type and length, which produces minimum M is the optimum window according to this criterion.
5. $M_{\min}$ is the best energy concentration measure obtained for the optimum window, and $(\sigma_{t_{\text{opt}}})_M$ is the optimum standard deviation of window in time for minimum M.

Table 1 Simulation results for different cases in STGTFT domain for single-component quadratic chirp

Parameters	Case 1 $a = 0$ and $\alpha \neq 90° \neq \alpha_{opt}$		Case2 $a \neq 0$ and $\alpha = 90° \neq \alpha_{\text{opt}}$		Case 3 $a \neq 0$ and $\alpha \neq \alpha_{\text{opt}}$		Case 4 $a \in (-\infty, \infty)$ and $\alpha = \alpha_{\text{opt}}$	
τ (sec)	1	1	1	2	1	2	1	2
a (Hz^2)	0	0	100	150	-100	100	100	50
f_s (Hz)	400	800	400	800	400	800	400	600
N	400	800	400	1600	400	1600	400	1200
f_d (Hz)	20	30	0	20	30	20	10	10
c (Hz^3)	10	10	10	10	10	20	10	5
α	72°	27°	90°	90°	−72°	−72°	82.37°	85.23°
α_{opt}	90°	90°	82.87°	79.38°	−82.87°	82.87°	82.87°	85.23°
$Mean\ \sigma_{t_{\text{opt}}}$	10	6	17	27	14	17	44	125
$Est.\sigma_{t_{\text{opt}}}$	9.89	5.7	15.96	26.06	12.61	16.82	40	120
$Mean\ (\sigma_{\alpha'})_{\min}$	3.79	6.9	2.41	6.52	2.99	9.79	0.55	0.56
$Est.\ (\sigma_{\alpha'})_{\min}$	4.32	7.18	2.82	6.90	3.40	10.18	0.789	0.793
$M_{\min}$	$6.66 * 10^3$	$2.08 * 10^4$	$4.67 * 10^3$	$4.22 * 10^4$	$5.39 * 10^3$	$6.03 * 10^4$	$2.16 * 10^3$	$7.48 * 10^3$
$(\sigma_{t_{\text{opt}}})_M$	10	6	16	26	12	17	42	115

Based on Table 1, we can observe that case 4 has the least mean $(\sigma_{\alpha'})_{\min}$ standard deviation in the cubic-matched in the cubic-matched ck-STGTFT domain and it is less than unity as derived in Eq. (60). This condition is equivalent to matched ck-STGTFT. Hence, AGFS produces least variance and high concentrated spectrogram at matched ck-STGTFT ($f_0^3\lambda = c\ and\ \alpha = \alpha_{\text{opt}}$) and optimum window length. We also note that $(\sigma_{t_{\text{opt}}})_M$ and $Mean\ \sigma_{t_{\text{opt}}}$ match significantly in Table 1, implying that the optimum window length found by 3 sigma rule for Gaussian window is also close to optimum window length according to the ECM criterion.

5 Uncertainty of the STGTFT

The uncertainty of the STGTFT can be derived in a manner similar to the STFT [15] and the STFrFT [46]. It yields the same result as the STFrFT, as shown in the next section. Subsequently, the TBP for the special case of quadratic chirp analysed by cubic kernel STGTFT is presented as an example.

5.1 2D Resolution of STGTFT

The 2D resolution of STGTFT is similar to the 2D resolution of GTFT at any particular instant of time t. When a window is sliding, multiple 2D GTFT resolution cells can be obtained at different instants of time t. The GTFT TBP is greater than or equal to $|\sin\alpha|/2$ as obtained in [37]. Therefore, the 2D resolution of GTFT is equal to reciprocal of the TBP of GTFT, which is always less than or equal to $2/|\sin\alpha|$. So the 2D resolution of STGTFT at any particular instant of time t is always less than or equal to $2/|\sin\alpha|$.

5.2 TBP of STGTFT

The STGTFT is defined over the domain of two variables. We would like to know the spread of this function over both of these variables. For any given input signal, most of the energy of the STGTFT lies within a rectangle on the time-GTFT frequency plane. The product of two sides of this rectangle can be considered as a measure of support (also known as the time-GTFT bandwidth product (TGBP)) [30].

We define the mean time ($\bar{t_S}$), mean GTFT frequency ($\bar{f_S}$), time width (T_S^2) and GTFT-bandwidth ($B_{S,\alpha,\lambda}^2$) of the STGTFT as follows:

$$\bar{t_S} = \frac{1}{||X_{\alpha,\lambda}^g(t,f)||^2} \iint_{-\infty}^{+\infty} t|X_{\alpha,\lambda}^g(t,f)|^2 \mathrm{d}t\mathrm{d}f, \tag{62}$$

$$\bar{f_S} = \frac{1}{||X_{\alpha,\lambda}^g(t,f)||^2} \iint_{-\infty}^{+\infty} f|X_{\alpha,\lambda}^g(t,f)|^2 \mathrm{d}t\mathrm{d}f, \tag{63}$$

$$T_S^2 = \frac{1}{||X_{\alpha,\lambda}^g(t,f)||^2} \iint_{-\infty}^{+\infty} (t-\bar{t_S})^2|X_{\alpha,\lambda}^g(t,f)|^2 \mathrm{d}t\mathrm{d}f, \tag{64}$$

$$B_{S,\alpha,\lambda}^2 = \frac{1}{||X_{\alpha,\lambda}^g(t,f)||^2} \iint_{-\infty}^{+\infty} (f-\bar{f_S})^2|X_{\alpha,\lambda}^g(t,f)|^2 \mathrm{d}t\mathrm{d}f. \tag{65}$$

For the original signal $x(t)$, the mean-time ($\bar{t_x}$), mean GTFT frequency ($\bar{f_x}$), time width (T_x^2) and GTFT bandwidth ($B_{x,\alpha,\lambda}^2$) are considered as per standard definitions. Also for the window function $g(t)$, mean-time ($\bar{t_g}$), mean frequency ($\bar{f_g}$), time width

(T_g^2) and bandwidth (B_g^2) are similarly considered as per standard definitions. It can be proved that

$$\bar{t_S} = \bar{t_x} - \bar{t_g}, \tag{66}$$

$$\bar{f_S} = \bar{f_x} - \bar{f_g}, \tag{67}$$

$$T_S^2 = T_x^2 + T_g^2 - \bar{t_S}^2 - 2\bar{t_x}\bar{t_g}, \tag{68}$$

$$B_{S,\alpha,\lambda}^2 = B_{x,\alpha,\lambda}^2 + B_g^2 \sin^2\alpha - \bar{f_x}^2 - \bar{f_g}^2. \tag{69}$$

It can be shown that a Gaussian window leads to the maximum 2D resolution. We consider a unit energy Gaussian window as

$$g(\tau) = (\pi\sigma^2)^{-1/4} \mathrm{e}^{-\tau^2/2\sigma^2}. \tag{70}$$

Its squared time width and bandwidth are

$$T_g^2 = \frac{\sigma^2}{2}, \tag{71}$$

$$B_g^2 = \frac{1}{2\sigma^2}. \tag{72}$$

If $x(t)$ and $g(t)$ are real and zero mean, then $\bar{f_x} = \bar{f_g} = \bar{t_x} = \bar{t_g} = 0$. Hence, the time-GTFT bandwidth product is given by

$$\mathrm{TGBP}_{S,\alpha,\lambda}^2 = T_S^2 B_{S,\alpha,\lambda}^2 = T_x^2 B_{x,\alpha,\lambda}^2 + \frac{1}{2\sigma^2} T_x^2 \sin^2\alpha + \frac{\sigma^2}{2} B_{x,\alpha,\lambda}^2 + \frac{1}{4}\sin^2\alpha. \tag{73}$$

By the AM-GM inequality,

$$\begin{aligned} \mathrm{TGBP}_{S,\alpha,\lambda}^2 \geq & T_x^2 B_{x,\alpha,\lambda}^2 + \frac{1}{4}\sin^2\alpha + 2\sqrt{\frac{1}{2\sigma^2} T_x^2 \sin^2\alpha . \frac{\sigma^2}{2} B_{x,\alpha,\lambda}^2} \\ = & \left(T_x B_{x,\alpha,\lambda} + \frac{1}{2}|\sin\alpha| \right)^2. \end{aligned} \tag{74}$$

This equality is attained if and only if

$$\sigma^2 = \frac{T_x |\sin\alpha|}{B_{x,\alpha,\lambda}}. \tag{75}$$

Therefore, for minimum GTFT domain support, the optimal STGTFT is obtained by using the Gaussian window

$$g(\tau) = \left(\pi \frac{T_x |\sin\alpha|}{B_{x,\alpha,\lambda}} \right)^{-1/4} \exp\left(-\frac{B_{x,\alpha,\lambda} \cdot \tau^2}{2T_x |\sin\alpha|} \right), \tag{76}$$

where $\alpha \neq k\pi$, $k \in \mathbb{Z}$. This will also ensure maximum 2D resolution.

5.3 Uncertainty in the Case of a Cubic Signal Analysed by ck - STGTFT

For the signal $x(\tau)$ and unit energy Gaussian window function $g(\tau)$ given by Eq. (38) and Eq. (39), we can construct the windowed signal $h_t(\tau)$ and its L^2 normalised version $\eta_t(\tau)$ as

$$h_t(\tau) = x(\tau)g(\tau - t), \tag{77}$$

$$\eta_t(\tau) = \frac{h_t(\tau)}{||h_t(\tau)||_2} = (\pi\sigma_{t_0}^2)^{-\frac{1}{4}} \exp\left(-\frac{(\tau-t)^2}{2\sigma_{t_0}^2}\right) \exp\left(i\pi c\tau^3 + i\pi a\tau^2 + i2\pi f_d\tau\right), \tag{78}$$

where $||h_t(\tau)||_2$ is L^2 normalisation of the signal $h_t(\tau)$. Then, the mean time ($\bar{t_s}$) and variance (T_s^2) of this signal can be calculated as:

$$\bar{t_s} = \int_{-\infty}^{+\infty} \tau|\eta_t(\tau)|^2 d\tau = t, \tag{79}$$

$$T_s^2 = \int_{-\infty}^{+\infty} (\tau - \bar{t_s})^2|\eta_t(\tau)|^2 d\tau = \frac{\sigma_t^2}{2}. \tag{80}$$

Similarly, the frequency centre (Ω_s) and frequency variance (B_s^2) can also be calculated as (see electronic supplementary material section 8 for detailed derivation of frequency centre and frequency variance)

$$\begin{aligned}\Omega_s &= \int_{-\infty}^{+\infty} \Omega|N_{t,\alpha,\lambda}(\Omega)|^2 \mathrm{d}\Omega \\ &= -i\sin\alpha \int_{-\infty}^{+\infty} \eta_t^*(\tau_2) \exp\left[-i\pi f_0^2\tau_2^2\cot\alpha + i\pi f_0^3\lambda\tau_2^3\right] \\ &\qquad \frac{\partial}{\partial\tau_2}\left(\eta_t(\tau_2)\exp\left[i\pi f_0^2\tau_2^2\cot\alpha - i\pi f_0^3\lambda\tau_2^3\right]\right)\mathrm{d}\tau_2,\end{aligned} \tag{81}$$

where $N_{t,\alpha,\lambda}(\Omega)$ is ck-GTFT of $\eta_t(\tau)$. Substituting $\eta_t(\tau)$ from Eq. (78) in the above expression and evaluating the integral, we obtain

$$\Omega_s = \sin\alpha\left[2\pi\left(f_d + (a + f_0^2\cot\alpha)t\right) + 3\pi(c - f_0^3\lambda)\left(t^2 + \frac{\sigma_t^2}{2}\right)\right]. \tag{82}$$

For frequency variance,

$$\begin{aligned}B_s^2 &= \int_{-\infty}^{+\infty} (\Omega - \Omega_s)^2\,|N_{t,\alpha,\lambda}(\Omega)|^2 \mathrm{d}\Omega = \int_{-\infty}^{+\infty} \Omega^2|N_{t,\alpha,\lambda}(\Omega)|^2 d\Omega - \Omega_s^2 \\ &= -\sin^2\alpha \int_{-\infty}^{+\infty} \eta_t^*(\tau_2)\exp\left[-i\pi f_0^2\tau_2^2\cot\alpha + i\pi f_0^3\lambda\tau_2^3\right] \\ &\qquad \cdot \frac{\partial^2}{\partial\tau_2^2}\left(\eta_t(\tau_2)\exp\left[i\pi f_0^2\tau_2^2\cot\alpha - i\pi f_0^3\lambda\tau_2^3\right]\right)\mathrm{d}\tau_2 - \Omega_s^2.\end{aligned} \tag{83}$$

Substituting $\eta_t(\tau)$ from Eq. (78) in the above expression and evaluating the integral, we obtain

$$B_s^2 = \frac{\sin^2\alpha}{2\sigma_t^2}\left[4\pi^2\sigma_t^4\left((a + f_0^2\cot\alpha) + 3t(c - f_0^3\lambda)\right)^2 + 9\pi^2\sigma_t^6(c - f_0^3\lambda)^2 + 1\right]. \tag{84}$$

5.3.1 TBP of Quadratic Signal Using ck-STGTFT, STFrFT and STFT

From Eq. (80) and Eq. (84), the TBP in STGTFT domain can be stated as follows:

$$\begin{aligned} TBP^2_{\text{STGTFT}} &= T_s^2 B_s^2 \\ &= \frac{\sin^2\alpha}{4}\left[4\pi^2\sigma_t^4\left((a + f_0^2\cot\alpha) + 3t(c - f_0^3\lambda)c\right)^2\right. \\ &\qquad \left. + 9\pi^2\sigma_t^6(c - f_0^3\lambda)^2 + 1\right]. \end{aligned} \tag{85}$$

The following cases can be inferred from Eq. (85):

– Case 1: Quadratic chirp analysed using STFT ($\alpha = 90°$, $\lambda = 0$):

$$TBP^2_{STFT} = \frac{1}{4}\left[4\pi^2\sigma_t^4\,(a + 3ct)^2 + 9\pi^2\sigma_t^6c^2 + 1\right]. \tag{86}$$

– Case 2: Quadratic chirp analysed using matched STFrFT ($\cot\alpha_{\text{opt}} = -a/f_0^2$, $\lambda = 0$):

$$\begin{aligned} TBP^2_{\text{STFrFT}} &= \frac{f_0^4}{4(f_0^4 + a^2)}\left[36\pi^2\sigma_t^4t^2c^2 + 9\pi^2\sigma_t^6c^2 + 1\right] \\ &= \frac{\sin^2\alpha}{4}\left[36\pi^2\sigma_t^4t^2c^2 + 9\pi^2\sigma_t^6c^2 + 1\right]. \end{aligned} \tag{87}$$

– Case 3: Quadratic chirp analysed using matched ck-STGTFT ($\cot\alpha = -a/f_0^2$, $f_0^3\lambda = c$):

$$TBP^2_{\text{ck}-\text{STGTFT}} = \frac{f_0^4}{4(f_0^4 + a^2)} = \frac{\sin^2\alpha}{4}. \tag{88}$$

Hence, it can be clearly seen that the following inequality holds as

$$TBP^2_{\text{STFT}} \geq TBP^2_{\text{STFrFT}} \geq TBP^2_{\text{ck}-\text{STGTFT}}. \tag{89}$$

In the case of quadratic chirp (non-zero 'a' and 'c'), these inequalities are strict. Hence, it is evident that for a quadratic chirp, the matched ck-STGTFT has the most compact support.

As shown in Eq. (88) and Eq. (89), TBP of ck-STGTFT is always greater than or equal to $|\sin\alpha|/2$. So TBP of ck-STGTFT at matched condition for a quadratic chirp is equal to TBP of fractional Fourier transform at matched condition for a linear chirp, which is equal to $|\sin\alpha|/2$ [40].

5.3.2 TBP Comparison of ck-STGTFT with TBP of Fractional Fourier Ambiguity Function, and Fractional Fourier Wigner-Ville Distribution

R. Tao et al. [47] and Tian-Wen Che et al. [12] proposed an ambiguity function (AF) based on the linear canonical transform (LCT) to estimate parameters of the quadratic signal. Similarly, WVD based on LCT has been proposed and used for the estimation of quadratic signal parameters [32, 41]. LCT kernel is a generalisation of FrFT, and it is a quadratic transform.

– Fractional Fourier based AF (FrAF) associated with FrFT or LCT is defined as

$$\mathrm{FrAF}_{x(t),\alpha}(\tau, f) = \int_{-\infty}^{\infty} x(t+\tau/2)x^*(t-\tau/2)K_\alpha(t, f)\mathrm{d}t. \tag{90}$$

– Fractional Fourier based WVD (FrWVD) associated with FrFT or LCT (FrWVD) is defined as

$$\mathrm{FrWDF}_{x(t),\alpha}(t, f) = \int_{-\infty}^{\infty} x(t+\tau/2)x^*(t-\tau/2)K_\alpha(\tau, f)\mathrm{d}\tau. \tag{91}$$

Uncertainty Principle for FrAF: Consider a unit energy signal $x(t)$ and its FrFT $X_\alpha(f)$. Let τ_{mean} be mean time and f_{mean} be mean frequency of the signal $x(t)$.

$$\int_{-\infty}^{\infty} |x(\tau)|^2\mathrm{d}\tau = 1 \text{ and } \int_{-\infty}^{\infty} |X_\alpha(f)|^2\mathrm{d}f = 1,$$
$$\int_{-\infty}^{\infty} \tau|x(\tau)|^2\mathrm{d}\tau = \tau_{\text{mean}} \text{ and } \int_{-\infty}^{\infty} f|X_\alpha(f)|^2\mathrm{d}f = f_{\text{mean}}.$$

Now consider time variance of FrAF is $\sigma^2_{t_{FrAF}}$

$$\begin{aligned}
\sigma^2_{t_{FrAF}} &= \iint_{-\infty}^{\infty} (\tau-\tau_{\text{mean}})^2 |AF^G_{x(t),\alpha}(\tau, f)|^2\mathrm{d}\tau\mathrm{d}f, \\
&= \int_{-\infty}^{\infty} (\tau-\tau_{\text{mean}})^2 \int_{-\infty}^{\infty}\int_{-\infty}^{\infty} x(t+\tau/2)x^*(t-\tau/2) \\
&\qquad x^*(t'+\tau/2)x(t'-\tau/2)\left[\int_{-\infty}^{\infty} K_\alpha(t, f)^* K_\alpha(t', f)\mathrm{d}f\right]\mathrm{d}t\mathrm{d}t'\mathrm{d}\tau, \\
&= \iint_{-\infty}^{\infty} (\tau-\tau_{\text{mean}})^2 |x(t+\tau/2)|^2 |x(t-\tau/2)|^2\mathrm{d}\tau\mathrm{d}t.
\end{aligned}$$

Put $t + \tau/2 = m$, $t - \tau/2 = n$, If $x(t)$ is real and zero mean, then $\tau_{\text{mean}} = 0$. Hence, the time-variance is given

$$\sigma^2_{t_{FrAF}} = \iint_{-\infty}^{\infty} (m-n)^2 |x(m)|^2 |x(n)|^2 \mathrm{d}m\mathrm{d}n = 2\int_{-\infty}^{\infty} m^2 |x(m)|^2 \mathrm{d}m. \tag{92}$$

Now consider frequency variance of FrAF is $\sigma^2_{f_{FrAF}}$

$$\begin{aligned}
\sigma^2_{f_{FrAF}} &= \iint_{-\infty}^{\infty} (f - f_{\text{mean}})^2 |AF^G_{X_\alpha(u),\alpha}(f,\tau)|^2 \mathrm{d}\tau\mathrm{d}f, \\
&= \int_{-\infty}^{\infty} (f - f_{\text{mean}})^2 \int_{-\infty}^{\infty} X_\alpha(u + f/2) X^*_\alpha(u - f/2) \\
&\quad \int_{-\infty}^{\infty} X^*_\alpha(u' + f/2) X_\alpha(u' - f/2). \left[\int_{-\infty}^{\infty} K_\alpha(u,\tau)^* K_\alpha(u',\tau)\mathrm{d}\tau\right] \mathrm{d}u\mathrm{d}u'\mathrm{d}f, \\
&= \iint_{-\infty}^{\infty} (f - f_{\text{mean}})^2 |X_\alpha(u + f/2)|^2 |X_\alpha(u - f/2)|^2 \mathrm{d}u\mathrm{d}f.
\end{aligned}$$

Put $u + f/2 = w$, $u - f/2 = v$, If $x(t)$ is real and zero mean, then $f_{\text{mean}} = 0$. Hence, the frequency-variance is given

$$\sigma^2_{f_{FrAF}} = \iint_{-\infty}^{\infty} (w-v)^2 |X_\alpha(w)|^2 |X_\alpha(v)|^2 \mathrm{d}w\mathrm{d}v = 2\int_{-\infty}^{\infty} w^2 |X_\alpha(w)|^2 \mathrm{d}w. \tag{93}$$

From Eq. (92) and Eq. (93), square of time bandwidth product can be written

$$\sigma^2_{t_{FrAF}} \sigma^2_{f_{FrAF}} = 4\int_{-\infty}^{\infty} m^2 |x(m)|^2 \mathrm{d}m \int_{-\infty}^{\infty} w^2 |X_\alpha(w)|^2 \mathrm{d}w = 4 \cdot \sigma^2_{t_{GTFT}} \sigma^2_{f_{GTFT}},$$

where $\sigma^2_{t_{FrFT}}$ is time variance and $\sigma^2_{f_{FrFT}}$ is frequency variance of FrAF and their product is always greater than or equal to $\sin^2 \alpha/4$ [40].

$$\begin{aligned}
\sigma^2_{t_{FrAF}} \cdot \sigma^2_{f_{FrAF}} &\geq 4 \cdot \frac{\sin^2 \alpha}{4}. \\
\therefore \sigma_{t_{FrAF}} \cdot \sigma_{f_{FrAF}} &\geq |\sin \alpha|.
\end{aligned} \tag{94}$$

Uncertainty Principle for FrWVD: we can also derive the uncertainty principle or TBP for FrWVD.

$$\sigma_{t_{FrWVD}} \cdot \sigma_{f_{FrWVD}} \geq \frac{|\sin \alpha|}{4}. \tag{95}$$

where $\sigma^2_{t_{FrWVD}}$ is time variance, and $\sigma^2_{f_{FrWVD}}$ is frequency variance of FrWVD.

As shown in Eq. (95), TBP of FrWVD for quadratic chirp is always greater than or equal to $|\sin \alpha|/4$. So FrWVD gives the least lower bound of TBP for a quadratic

chirp. However, it produces cross-term in the presence of a multicomponent signal, and it is not possible to remove cross-terms without compromising the resolution of signal representation [15]. Similarly, as shown in Eq. (94), TBP of FrAF is always greater than or equal to $|\sin\alpha|$. So FrAF gives higher lower bound of TBP as compared to the lower bound of TBP of ck-STGTFT for the representation of quadratic chirp and produces cross-terms in multicomponent signal analysis. Hence, it can be concluded that the following inequality holds for the lower bounds of TBP, or least uncertainty, in case of monocomponent quadratic chirp as

$$LTBP^2_{FrAF} \geq LTBP^2_{ck-STGTFT} \geq LTBP^2_{FrWVD}, \tag{96}$$

where $LTBP$ is lower bound of time bandwidth product.

6 ck-AGFS Performance Compared to Existing TFDs

To demonstrate the effectiveness of ck-AGFS, two close amplitude modulated quadratic chirps are considered.

$$\begin{aligned} x_1(t) &= \begin{cases} e^{i\pi c_1 t^3 + i\pi a_1 t^2 + 2i\pi f_{d1}} & 0 \leq t < 2\text{sec} \\ e^{i\pi c_2 t^3 + i\pi a_2 t^2 + 2i\pi f_{d2}} & 2 \leq t < 4\text{sec} \end{cases}, \\ x_2(t) &= \begin{cases} e^{i\pi c_3 t^3 + i\pi a_3 t^2 + 2i\pi f_{d3}} & 0 \leq t < 2\text{sec} \\ e^{i\pi c_4 t^3 + i\pi a_4 t^2 + 2i\pi f_{d4}} & 2 \leq t < 4\text{sec} \end{cases}, \end{aligned} \tag{97}$$

$$x(t) = 2e^{-0.08t} \cdot x_1(t) + 1.5e^{-0.04t} \cdot x_2(t). \tag{98}$$

Here we consider $c_1 = c_3$, $c_2 = c_4$, $a_1 = a_3$ and $a_2 = a_4$. Signal parameters (quadratic rate, chirp rate and Doppler frequency) of both components change in between the signal duration. Parameters of simulated quadratic chirps are mentioned in Table 2. Fig. 1(a) shows ck-AGFS of quadratic chirp with approximate confined Gaussian

Table 2 Simulation parameter of $x(t)$ for amplitude modulated quadratic chirps

Amplitude modulated quadratic chirps parameters									
τ (sec)	f_s (Hz)	$c_1(Hz^3)$	$a_1(Hz^2)$	f_{d1} (Hz)	f_{d2} (Hz)	$c_2(Hz^3)$	$a_2(Hz^2)$	f_{d3} (Hz)	f_{d4}(Hz)
4	1200	5	50	20	15	10	25	80	75

window (ACGW) used. ACGW produces least frequency domain variance among all the windows with given time domain variance [43]. Optimum Gaussian window length of AGFS is 480 samples as per Eq. (59), and estimated matched angle is 85.23° for $0 \leq t < 2$ seconds and 87.61° for $2 \leq t < 4$ seconds. It is observed that analysis with ACGW window produces marginally less spread in the frequency domain than using a Gaussian window. Fig. 1(b) shows the STFT based spectrogram of quadratic chirp, and its optimum window length of 64 samples. Fig. 1(c-l) show the STFrFT based TFD, the quadratic WVD (QWVD) based TFD, the fourth order polynomial

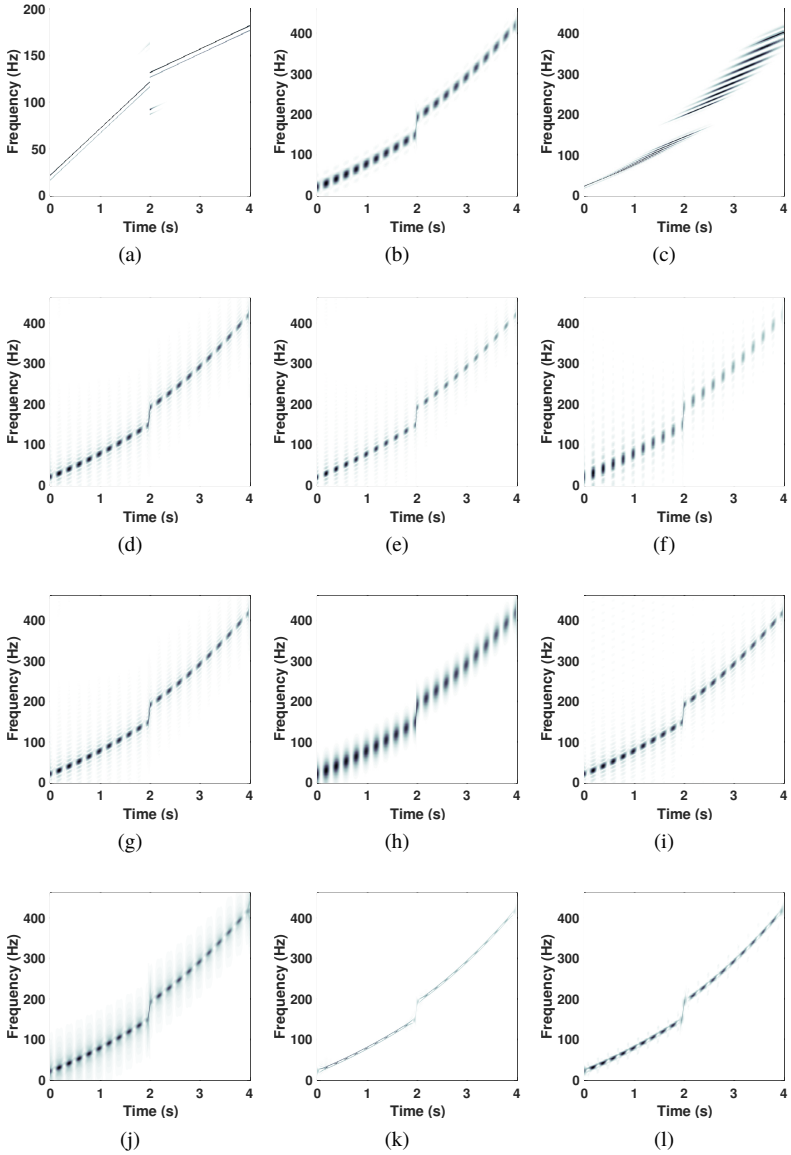

Fig. 1 Comparison of different TFDs with ck-AGFS for multicomponent quadratic chirp (a) ck-AGFS (b) STFT (c) STFrFT (d) QWVD (e) PWVD4 (f) PWVD6 (g) MBD (h) EMBD (i) CW (j) AFS (k) CKD (l) AOK

WVD (PWVD4) based TFD, the sixth order polynomial WVD (PWVD6) based TFD, modified B distribution (MBD), extended modified B distribution (EMBD), Choi–Williams (CW) distribution, adaptive fractional spectrogram (AFS), compact kernel distribution (CKD), and adaptive orthogonal kernel (AOK) respectively.

We can see from Fig. 1 that all other TFDs except AGFS are unable to represent two different nearby chirp signals distinguishably in the TF plane. Similarly Fig. 2 shows time slices of AGFS and other TFDs at time instant of 1 second and it shows that none of TFD except AGFS is capable to represent two peaks separately. This shows the superiority of ck-AGFS over other TFDs to resolve two nearby amplitude modulated quadratic chirps. Hence, AGFS has higher resolution than the existing TFDs. Mathematical results of uncertainty principle in Eq. (89) was also evident in simulation results shown in Fig. 1(a) of AGFS, Fig. 1(b) of STFT based TFD and Fig. 1(c) of STFrFT based TFD for representation of multicomponent quadratic chirp.

ECM values as per Eq. (61) are also computed for all TFDs for multicomponent signal given by Eq. (97) and are reported in the Table 3. The least M value is obtained for ck-AGFS, indicating that it is the highest concentration TFD among all the TFDs.

Table 3 Comparison of energy concentration measurement (ECM) of different TFDs

TFD	**ck-AGFS**	STFrFT	STFT	QWVD	PWVD4	PWVD6
M	$\mathbf{1.29 * 10^5}$	$5.74 * 10^5$	$4.51 * 10^5$	$1.16 * 10^6$	$1.81 * 10^6$	$3.51 * 10^5$
TFD	MBD	EMBD	CW	CK TFD	AFS	AOK-TFD
M	$1.16 * 10^6$	$4.22 * 10^5$	$1.15 * 10^6$	$7.32 * 10^5$	$6.74 * 10^6$	$2.96 * 10^5$

To quantitatively measure the resolution of AGFS, Boashash-Sucic resolution measure [7, pp. 412-418] is used. For a time slice of the multicomponent signal at a time instant t, it is given as

$$P(t) = 1 - \frac{1}{3}\left[\left|\frac{A_s(t)}{A_m(t)}\right| + \frac{1}{2}\left|\frac{A_x(t)}{A_m(t)}\right| + \left(1 - \frac{S(t)}{D(t)}\right)\right], \tag{99}$$

where, for a pair of signal components, $A_m(t)$ is average amplitudes of the components' main-lobes; $A_s(t)$ is the average amplitudes of the components' side-lobes; $A_x(t)$ is the cross-term amplitude; $S(t)$ is the separation measure; and $D(t)$ is frequency separation of components' main-lobes. A high resolution TFD has a P value closer to 1, whereas a low resolution TFD has a P value closer to 0. The Boashash-Sucic resolution measure (P) is calculated for ck-AGFS of signal given by Eq. (97) at different time instants t and it is reported in Table 4. Least M value of AGFS from Table 3 indicates that AGFS

Table 4 Boashash-Sucic resolution measure (P) at different time instants of ck-AGFS

$t\ (s)$	A_m	A_s	A_x	S	D	**P**
1	0.68	0.019	0.012	9	10	**0.9577**
3	0.78	0.018	0.011	9	10	**0.9565**

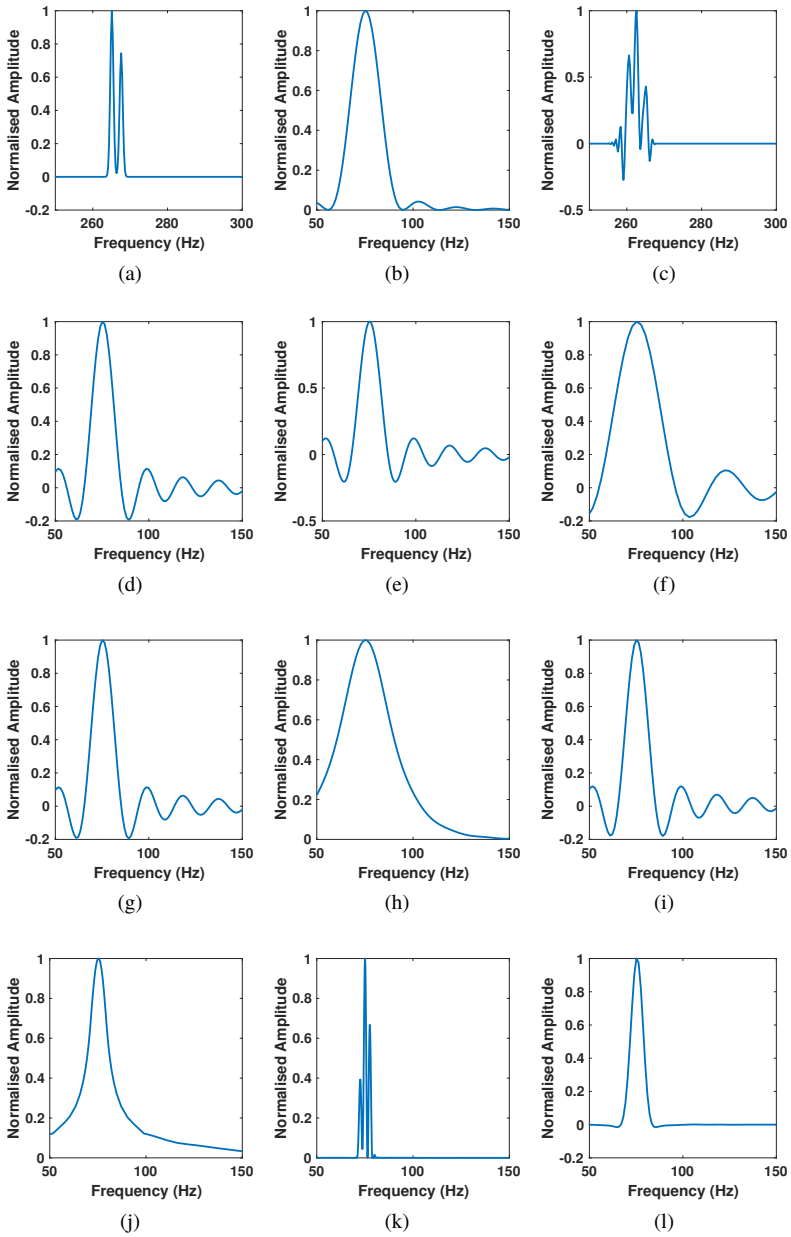

Fig. 2 Comparison of time slice of different TFDs for multicomponent quadratic chirp (a) ck-AGFS (b) STFT (c) STFrFT (d) QWVD (e) PWVD4 (f) PWVD6 (g) MBD (h) EMBD (i) CW (j) AFS (k) CKD (l) AOK

is a highly concentrated TFD. From Table 4, we can see that AGFS is a high resolution TFD since P values are very close to 1. Fig. 1 and Fig. 2 illustrate the distinguishing capability of AGFS compared to other TFDs. From section 3.5.9, we can see that AGFS is also capable of providing cross-term free TFD if individual components of a multicomponent signal have non-overlapping STGTFTs. These criteria combined together prove that AGFS can provide high resolution, high concentration, cross-term free TFD for multicomponent frequency modulated signal.

7 Extraction of Individual Components from Multicomponent Quadratic Chirp Using ck-AGFS

The FrFT can be used to extract different components of a noisy mixture of linear chirps [51]. Since ck-AGFS has a third-order kernel, it can be used to extract components of a noisy mixture of quadratic chirps. To illustrate this, we consider a noisy version of the bi-component amplitude-modulated quadratic chirp signal $x(t)$ defined by Eq. (98). Hence, we have $y(t) = x(t) + n(t)$ with SNR = 0 dB. For extraction, multiple ck-AGFS (here, two) are used. Only one chirp is focused in respective ck-AGFS at matched condition ($c_k = f_0^3 \lambda_k$ and $a_k = -f_0^2 cot\alpha_k$, where k is the index of the chirp component). When ck-AGFS is matched, the time window variance is optimum only for the chirp component that is being matched. Four cases of variation of component chirp parameters are considered.

7.1 Case A: Chirps Differing Only in Their Doppler Frequency

In this case, $x(t)$ has $c_1 = c_2 = c_3 = c_4 = c$ and $a_1 = a_2 = a_3 = a_4 = a$ and different Doppler frequencies f_{d1}, f_{d2}, f_{d3}, and f_{d4}. Doppler frequencies of both components change in between the signal duration. Simulation parameters are shown in Table 5. Once the ck-AGFS is computed on the received composite noisy signal, as shown in Fig. 1, the extraction of an individual component can be performed using the component extraction procedure described in [6].

Table 5 Simulation parameters of two amplitude modulated quadratic chirps (different in terms of Doppler frequency) for extraction using ck-AGFS at its optimum window length and matched angle

Case A: Amplitude modulated chirps are separated only in Doppler							
τ (sec)	f_s (Hz)	$c(Hz^3)$	$a(Hz^2)$	f_{d1}(Hz)	f_{d2}(Hz)	f_{d3}(Hz)	f_{d4}(Hz)
4	1200	5	50	20	15	80	75

Fig. 3(a) shows the STFT of the noisy signal with a window length of 64 samples, which clearly shows that the STFT is unable to resolve the two close components. Fig. 3(b) and Fig. 3(c) show the two ck-AGFS focused on each quadratic chirp component contained in the noisy received signal. The individual chirp components extracted

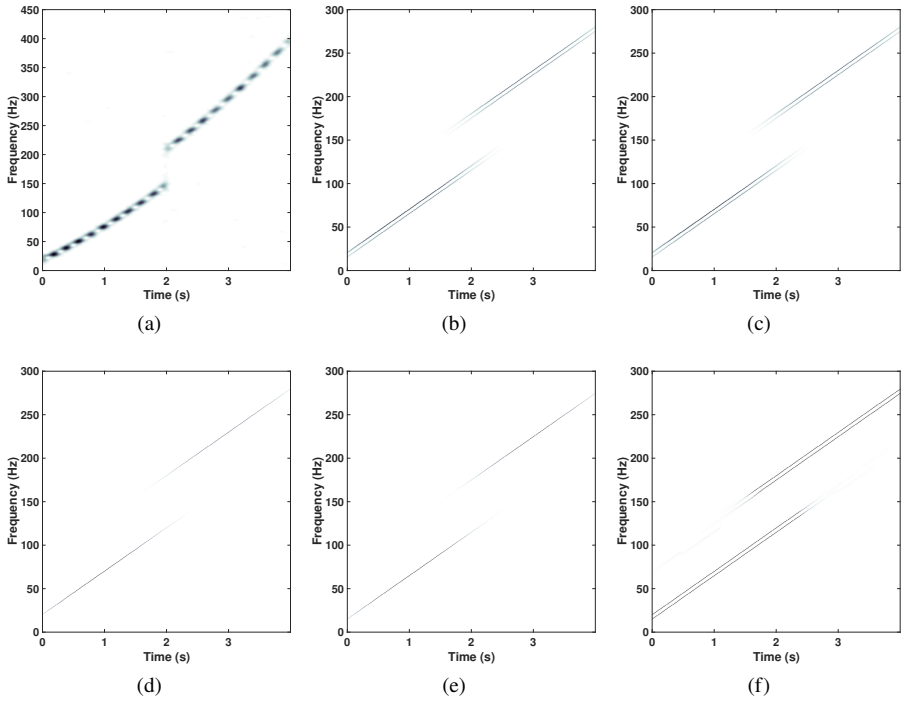

Fig. 3 Spectrogram view of extraction of mono-component quadratic chirp from multicomponent quadratic chirp (quadratic chirp differs in terms of Doppler frequency) using ck-AGFS algorithm (a) STFT spectrogram (b) AGFS focused on first component (c) AGFS focused on second component (d) Extracted first component (e) Extracted second component (f) AGFS fusion

using the algorithm described in [6] are shown in Fig. 3(d,e). The respective insignificant component (unfocused component) is zero padded to highlight the extracted component of interest. Fig. 3(f) shows the combined AGFS spectrogram obtained by combining the spectrograms of individual extracted components.

7.2 Case B: Chirps Differing Only in Their Chirp Rate

In this case, $x(t)$ has $c_1 = c_2 = c_3 = c_4 = c$ and $f_{d1} = f_{d2} = f_{d3} = f_{d4} = f_d$ and different chirp rates a_1, a_2, a_3, and a_4. Chirp rates of both components change in between the signal duration. Simulation parameters are shown in Table 6 for two quadratic chirps with different chirp rates. The subfigures of Fig. 4 respectively show the STFT spectrogram, AGFS focussed and extracted components and combined AGFS for this case using same procedure as in the previous case.

Table 6 Simulation parameters of two amplitude modulated quadratic chirps (which differ in terms of chirp rate) for extraction using ck-AGFS at its optimum window length and matched angle

Case B: Amplitude modulated chirps are separated only in Chirp Rates							
$\tau\ (s)$	$f_s\ (Hz)$	$c\ (Hz^3)$	$a_1\ (Hz^2)$	$a_2\ (Hz^2)$	$a_3\ (Hz^2)$	$a_4\ (Hz^2)$	$f_d\ (Hz)$
4	2500	5	200	190	180	170	20

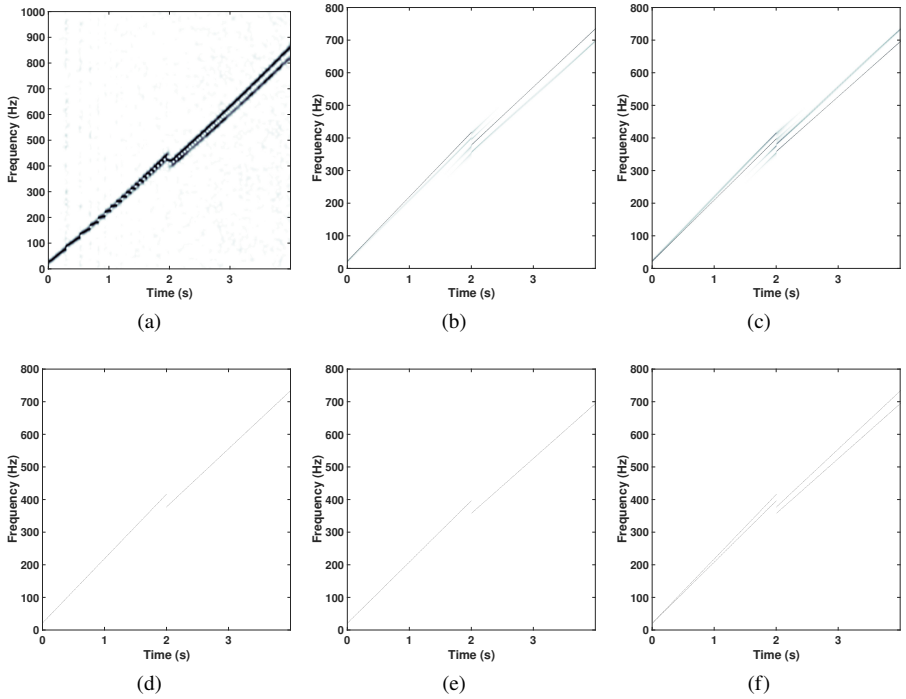

Fig. 4 Spectrogram view of extraction of mono-component quadratic chirp from multicomponent quadratic chirp (which differ in terms of chirp rate) using ck-AGFS algorithm (a) STFT spectrogram (b) AGFS focused on first component (c) AGFS focused on second component (d) Extracted first component (e) Extracted second component (f) AGFS fusion

7.3 Case C: Chirps Differing Only in Their Quadratic Rate

In this case, $x(t)$ has $a_1 = a_2 = a_3 = a_4 = a$ and $f_{d1} = f_{d2} = f_{d3} = f_{d4} = f_d$ and different quadratic rates c_1, c_2, c_3, and c_4. Quadratic rates of both components change in between the signal duration. Simulation parameters are shown in Table 7. The subfigures of Fig. 5 respectively show the STFT spectrogram, AGFS focussed and extracted components and combined AGFS for this case using same procedure as in the previous case.

Table 7 Simulation parameters of two amplitude modulated quadratic chirps (differ in terms of quadratic rates) for extraction using ck-AGFS at its optimum window length and matched angle

Case C: Amplitude modulated chirps are separated only in their Quadratic Rate								
$\tau\ (s)$	$f_s\ (Hz)$	$c_1\ (Hz^3)$	$c_2\ (Hz^3)$	$c_3\ (Hz^3)$	$c_4\ (Hz^3)$	$a\ (Hz^2)$	$f_{d1}\ (Hz)$	$f_{d2}\ (Hz)$
4	3000	5	15	25	35	25	30	10

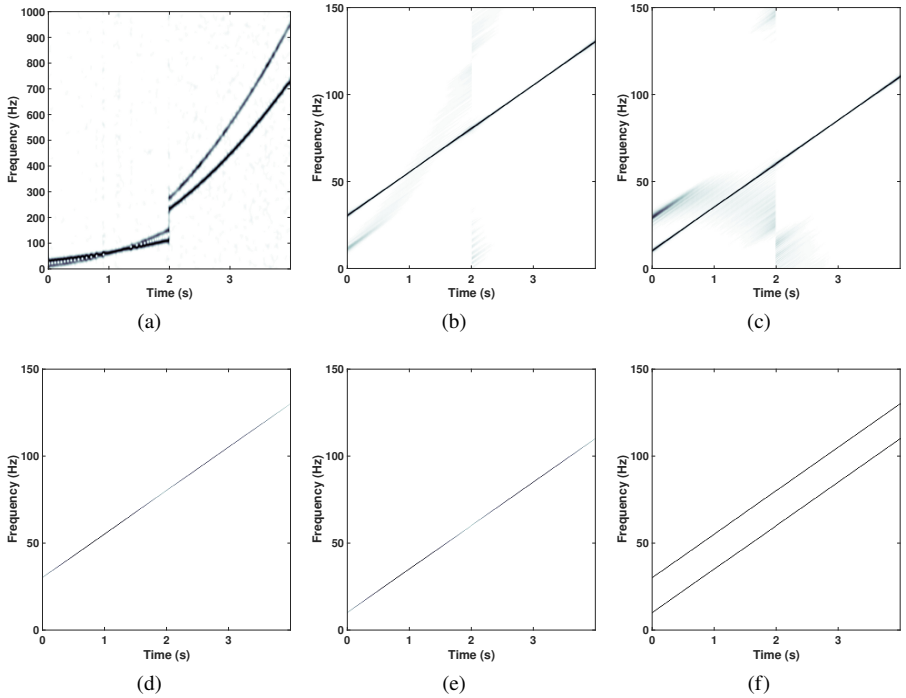

Fig. 5 Spectrogram view of extraction of mono-component quadratic chirp from multicomponent quadratic chirp (differ in terms of quadratic chirp rate) using ck-AGFS algorithm (a) STFT spectrogram (b) AGFS focused on first component (c) AGFS focused on second component (d) Extracted first component (e) Extracted second component (f) AGFS fusion

7.4 Case D: Crossed Chirps in Time-Frequency Domain

Here we demonstrate effectiveness of ck-AGFS in the special application of component extraction from a mixture of two quadratic chirps with different orientations crossing in their TFDs. Simulation parameters are shown in Table 8 for two different quadratic chirps at their matched GTFT of quadratic and cubic phase. The subfigures of Fig. 6 respectively show the STFT spectrogram, AGFS focused and extracted components and combined AGFS for this case using same procedure as in the previous case.

Table 8 Simulation parameters of two amplitude modulated quadratic chirps (crossed in time-frequency domain) for extraction using ck-AGFS at its optimum window length and matched angle

Case D. Amplitude modulated chirps are crossed in time-frequency domain						
$\tau\ (s)$	$f_s\ (Hz)$	$c_1\ (Hz^3)$	$c_2\ (Hz^3)$	$c_3\ (Hz^3)$	$c_4\ (Hz^3)$	$a_1\ (Hz^2)$
4	3000	5	8	9	12	100
$a_2\ (Hz^2)$	$a_3\ (Hz^2)$	$a_4\ (Hz^2)$	$f_{d1}\ (Hz)$	$f_{d2}\ (Hz)$	$f_{d3}\ (Hz)$	$f_{d4}\ (Hz)$
-200	50	-250	500	800	300	1180

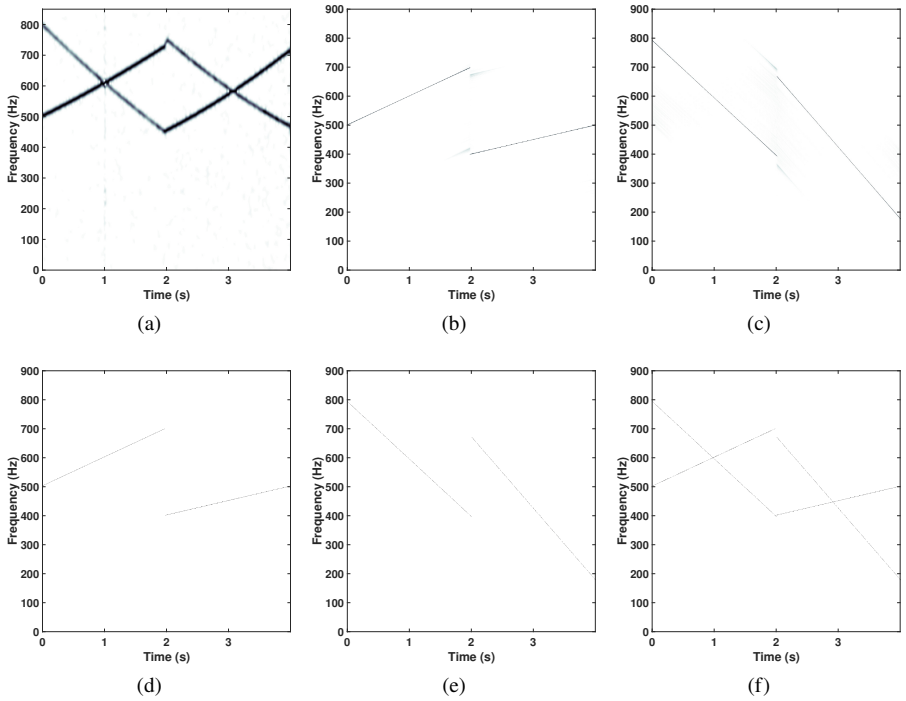

Fig. 6 Spectrogram view of extraction of mono-component quadratic chirp from multicomponent quadratic chirp (components cross in time-frequency domain) using ck-AGFS algorithm (a) STFT spectrogram (b) AGFS focused on first component (c) AGFS focused on second component (d) Extracted first component (e) Extracted second component (f) AGFS fusion

8 SNR gain and Mean Error Analysis of ck-AGFS

8.1 Cubic-Matched ck-STGTFT SNR Gain Analysis at Matched Cubic Phase Condition

Li et al [23] and Xia et al [49] proposed a definition of SNR, which is transform dependent and related directly to the bandwidth of the signal. Based on this, SNR in

cubic-matched ck-STGTFT domain can be defined as

$$SNR_{3dB}^{ck-STGTFT}(s(t)) = \frac{\frac{1}{B}\int_B |ck - STGTFT(s(t))|^2 \mathrm{d}t}{\sigma^2_{n,ck-STGTFT}}, \tag{100}$$

where $s(t)$ is the signal of interest, σ_n^2 is the variance of noise corrupting it, and B is the 3 dB bandwidth of $s(t)$ in the cubic-matched ck-STGTFT domain.

8.1.1 Mean (3dB) Signal Power in ck-STGTFT Domain

Eq. (45) was derived for the modulus of ck-STGTFT of a quadratic signal $x(t)$ given by Eq. (38). Using Eq.(46) and Eq. (45) , the maximum value of ck-STGTFT of a signal $x(t)$ is given by

$$\left|X^g_{\alpha,\lambda}(t,f)\right|^2_{\max} = \frac{|A|^2}{\sqrt{\pi\sigma^2_{\alpha 0}}}, \tag{101}$$

which occurs when $f = f^{'} = at\sin\alpha + f_d\sin\alpha + f_0^2 t\cos\alpha$. Therefore, the $3dB$ $|ck - STGTFT|$ value is half the maximum value which is given by

$$\left|X^g_{\alpha,\lambda}(t,f)\right|^2_{3\mathrm{dB}} = \frac{0.5|A|^2}{\sqrt{\pi\sigma^2_{\alpha 0}}}. \tag{102}$$

The upper and lower bounds of the frequency variable for this $3dB$ $|ck - STGTFT|$ value is given by

$$\underbrace{f^{'} - \sigma_{\alpha 0}\sqrt{ln2}}_{f_1} < f < \underbrace{f^{'} + \sigma_{\alpha 0}\sqrt{ln2}}_{f_2}. \tag{103}$$

Hence the mean value of the $|\mathrm{ck} - \mathrm{STGTFT}|^2$ over this interval is given by

$$\begin{aligned}\left\langle\left|X^g_{\alpha,\lambda}(t,f)\right|^2_{3\mathrm{dB}}\right\rangle &= \frac{1}{f_2 - f_1}\int_{f_1}^{f_2}\left|X^g_{\alpha,\lambda}(t,f)\right|^2 \mathrm{d}f,\\ &= \frac{B^2}{2\sigma_{\alpha 0}\sqrt{ln2}}\int_{f_1}^{f_2}\exp\left(-\frac{(f-f^{'})^2}{\sigma_{\alpha 0^2}}\right)\mathrm{d}f,\\ &= \frac{|A|^2}{\sqrt{\pi\sigma^2_{\alpha 0}}}\underbrace{\left(\frac{1}{\sqrt{ln2}}\int_0^{\sqrt{ln2}}\mathrm{e}^{-u^2}du\right)}_{\gamma\approx 0.8}.\end{aligned} \tag{104}$$

8.1.2 Noise Variance

The ck-STGTFT of noise, at cubic matched ck-STGTFT domain $f_0^3\lambda = c$ is given by

$$N_{\alpha,\lambda}(t,f) = \int_{-\infty}^{+\infty} n(\tau)g(\tau - t)K_{\alpha,\lambda=\frac{c}{f_0^3}}(\tau, f)\mathrm{d}\tau. \tag{105}$$

This noise variance in the cubic matched ck-STGTFT domain is given by

$$\sigma^2_{n,\text{ck}-\text{STGTFT}} = E\left[|N_{\alpha,\lambda}(t,f)|^2\right] = E\left[N_{\alpha,\lambda}(t,f)N^*_{\alpha,\lambda}(t,f)\right],$$

$$= \iint_{-\infty}^{+\infty} \overbrace{E\left[n(\tau_1)n^*(\tau_2)\right]}^{R_{nn}(\tau_1,\tau_2)} g(\tau_1 - t)g^*(\tau_2 - t)\cdot K_{\alpha,\lambda}(\tau_1, f)K^*_{\alpha,\lambda}(\tau_2, f)\mathrm{d}\tau_1\mathrm{d}\tau_2. \tag{106}$$

If we assume the noise to be additive white Gaussian noise (AWGN), the autocorrelation function is given by

$$R_{nn}(\tau_1, \tau_2) = \sigma_n^2\delta(\tau_1 - \tau_2)$$

Hence, the above integral collapses to

$$\begin{aligned}\sigma^2_{n,\text{ck}-\text{STGTFT}} &= \int_{-\infty}^{+\infty} \sigma_n^2 |g(\tau_1 - t)|^2 \underbrace{\left|K_{\alpha,\lambda}(\tau_1, f)\right|^2}_{|\text{cosec}\alpha|}\mathrm{d}\tau_1,\\ &= \sigma_n^2|\text{cosec}\alpha| \int_{-\infty}^{+\infty} |g(\tau_1 - t)|^2\,\mathrm{d}\tau_1,\\ &= \sigma_n^2 E_w|\text{cosec}\alpha|.\end{aligned}$$

Here, the window energy is unity ($E_w = 1$) by design (See Eq. (39)). Hence, the noise variance in ck-STGTFT domain:

$$\therefore \sigma^2_{n,\text{ck}-\text{STGTFT}} = \sigma_n^2|\text{cosec}\alpha|. \tag{107}$$

8.1.3 SNR gain Over Cubic-Matched ck-STGTFT Domain

Hence, the SNR in cubic matched ck-STGTFT domain is given by

$$\begin{aligned}\text{SNR}^{\text{ck}-\text{STGTFT}}_{\text{3dB}} &= \frac{\left\langle \left|X^g_{\alpha,\lambda}(t,f)\right|^2_{\text{3dB}} \right\rangle}{\sigma^2_{n,\text{ck}-\text{STGTFT}}}.\\ &= \frac{|A|^2\gamma\sin\alpha}{\sqrt{\pi}\sigma_{\alpha 0}\sigma_n^2} = \frac{\gamma\sin\alpha}{\sqrt{\pi}\sigma_{\alpha 0}}\cdot \text{SNR}_{\text{t}},\end{aligned} \tag{108}$$

where $\mathrm{SNR_t} = |A|^2/\sigma_n^2$ is the time domain SNR of the signal. Hence, the SNR gain is given by

$$\frac{\mathrm{SNR}_{\mathrm{3dB}}^{\mathrm{ck-STGTFT}}}{\mathrm{SNR_t}} = \frac{\gamma \sin\alpha}{\sqrt{\pi}\sigma_{\alpha 0}}. \tag{109}$$

This will be maximum for cubic phase matched STFT ($\alpha = 90°$). In case of cubic phase matched STFT, minimum Fourier domain variance $\sigma_{\alpha 0} = \sqrt{\frac{a}{\pi}}$ at optimum time variance $\sigma_{t_0} = \frac{1}{\sqrt{2\pi a}}$ is obtained using Eq. (46) , i.e [23][49]. In this case,

$$\max\left(\frac{\mathrm{SNR}_{\mathrm{3dB}}^{STFT}}{\mathrm{SNR_t}}\right) = \frac{\gamma}{\sqrt{a}}. \tag{110}$$

Similarly, maximum SNR gain is obtained using Eq. (46) for ck-STGTFT/ck-AGFS at $\alpha = \alpha_{\mathrm{opt}}$ (Optimal matched angle). In this case,

$$\max\left(\frac{SNR_{3dB}^{\mathrm{ck-STGTFT}}}{SNR_{\mathrm{t}}}\right) = 2\sqrt{\pi}\sigma_{t_0}\gamma. \tag{111}$$

If we consider a half-length $(N/2)$ sliding Gaussian window and $\gamma = 0.8$, then we obtain SNR gain of the discrete ck-STGTFT $\approx 0.57 \cdot N_1$, where N_1 is the sampling frequency multiplied by signal duration (T). In general, for a discrete multicomponent case, SNR gain of ck-STGTFT is given by

$$\frac{SNR^{\mathrm{ck-STGTFTdiscrete}}}{SNR_{\mathrm{t}}} \approx D_1\frac{N_0}{K}, \tag{112}$$

where D_1 is a constant, K is the number of components and N_0 is the number of samples within a window length [23][49].

8.2 GTFT SNR Gain Analysis

Consider a quadratic chirp signal $x(t)$ to be

$$x(t) = A\mathrm{e}^{i\pi ct^3 + i\pi at^2 + i2\pi f_d t}.$$

The GTFT of the signal x(t) is denoted by $X_{\alpha,\lambda}(f)$, and is defined as

$$\begin{aligned} X_{\alpha,\lambda}(f) = \int_{-\infty}^{+\infty} A \cdot \exp\big[&i\pi(c - f_0^3\lambda)t^3 + i\pi(a + f_0^2.\cot(\alpha))t^2 \\ &+ i2\pi(f_d - f\mathrm{cosec}(\alpha))t + i\pi t_0^2\cot(\alpha)f^2 + i\pi t_0^3\lambda f^3\big]\mathrm{d}t. \end{aligned} \tag{113}$$

The approximate analytical expression of GTFT magnitude spectrum $|X_{\alpha,\lambda}(f)|^2$ of $x(t)$ using the stationary phase approximation ($|f_d - f\mathrm{cosec}(\alpha)| >> 0$) for unmatched

cubic phase condition is given by

$$\left|X_{\alpha,\lambda}(f)\right|^2 \approx \frac{|A|^2|\text{cosec}\alpha|}{\sqrt{\left(a+f_0^2\cot\alpha\right)^2 - 6\left(c-f_0^3\lambda\right)(f_d - f\text{cosec}\alpha)}}$$
$$\cdot \cos^2\left(\frac{\pi\sqrt{\left(a+f_0^2\cot\alpha\right)^2 - 6\left(c-f_0^3\lambda\right)(f_d - f\text{cosec}\alpha)}}{27\left(c-f_0^3\lambda\right)^2}\right.$$
$$\left.\cdot\left[12\left(c-f_0^3\lambda\right)(f_d - f\text{cosec}\alpha) - 2\left(a+f_0^2\cot\alpha\right)^2\right] - \frac{\pi}{4}\right).$$

At GTFT matched condition ($c = f_0^3\lambda$ and $a = -f_0^2\cot\alpha$), response is an impulse at $f = f_d\sin\alpha$ with area $|A||A_\alpha|$, where $|A_\alpha|$ is the amplitude of GTFT kernel.

SNR gain analysis at GTFT matched condition is derived, considering $x(t)$ corrupted by AWGN $n(t)$ of variance σ_n^2. SNR of the signal $y(t) = x(t) + n(t)$ is given by [45][24][58]

$$\text{SNR}^{\text{GTFT}} = \frac{|\text{Peak signal power in GTFT domain}|_{f=f'}}{\text{Variance of output signal in GTFT domain}_{f=f'}},$$

where f' is the instant ($f' = f_d\sin\alpha$) where the maximum of numerator occurs. In general, GTFT uses the square modulus test, and test statistic can thus be taken as $|\text{GTFT}|^2$. Hence, the GTFT SNR is given by

$$\text{SNR}^{\text{GTFT}} = \frac{|GTFT_x|^4}{\text{Var}[|\text{GTFT}_\text{y}|^2]}, \tag{114}$$

where $|GTFT_x|$ is peak modulus of the signal $x(t)$ in GTFT domain and $|\text{GTFT}_\text{y}|$ is peak modulus of the signal $y(t)$ in GTFT domain. $\text{Var}|\text{GTFT}_\text{y}|^2$ can be written as

$$\text{Var}[|\text{GTFT}_\text{y}|^2] = E\left[\left|\text{GTFT}_\text{y}\right|^4\right] - E^2\left[\left|\text{GTFT}_\text{y}\right|^2\right]. \tag{115}$$

Since the signal and noise are uncorrelated, and noise is having zero mean,

$$E\left[\left|\text{GTFT}_\text{y}\right|^2\right] = \iint_{-\infty}^{+\infty} E\left([x(\tau_1)+n(\tau_1)]\,[x^*(\tau_2)+n^*(\tau_2)]\right)$$
$$\cdot K_{\alpha,\lambda}(\tau_1,f)K^*_{\alpha,\lambda}(\tau_2,f)\text{d}\tau_1\text{d}\tau_2.$$
$$\therefore E\left[\left|GTFT_y\right|^2\right] = |A|^2|A_\alpha|^2T^2 + \sigma_n^2|A_\alpha|^2T. \tag{116}$$

where T is the time duration of $x(t)$. Similarly,

$$E\left[\left|\mathrm{GTFT_y}\right|^4\right] = \iiiint_{-\infty}^{+\infty} E\big([x(\tau_1)+n(\tau_1)]\,[x(\tau_2)+n(\tau_2)]\,[x^*(\tau_3)+n^*(\tau_3)]$$
$$[x^*(\tau_4)+n^*(\tau_4)]\big)K_{\alpha,\lambda}(\tau_1,f)K_{\alpha,\lambda}(\tau_2,f)$$
$$K^*_{\alpha,\lambda}(\tau_3,f)K^*_{\alpha,\lambda}(\tau_4,f)\mathrm{d}\tau_1\mathrm{d}\tau_2\mathrm{d}\tau_3\mathrm{d}\tau_4.$$

$$\therefore E\left[\left|\mathrm{GTFT_y}\right|^4\right] = |A_\alpha|^4\left[|A|^4T^4 + 2T^2\sigma_n^4 + 4T^3|A|^2\sigma_n^2\right]. \tag{117}$$

Hence variance is given by

$$\mathrm{Var}|\mathrm{GTFT_y}|^2 = |A_\alpha|^4\left[\sigma_n^4T^2 + 2T^3|A|^2\sigma_n^2\right]. \tag{118}$$

Therefore, GTFT SNR and SNR gain are given by

$$\mathrm{SNR^{GTFT}} = \frac{|A_\alpha|^4|A|^4T^4}{|A_\alpha|^4\left[\sigma_n^4T^2 + 2T^3|A|^2\sigma_n^2\right]} = \frac{T^2\mathrm{SNR_t}^2}{2T\mathrm{SNR_t}+1}, \tag{119}$$

$$\frac{\mathrm{SNR^{GTFT}}}{\mathrm{SNR_t}} \approx \frac{T}{2}. \tag{120}$$

where SNR_t is input SNR, defined as A^2/σ_n^2. In discrete case, SNR gain is given by

$$\frac{\mathrm{SNR^{GTFTdiscrete}}}{\mathrm{SNR_t}} \approx D\frac{N}{K}, \tag{121}$$

where D is a constant, K is the number of components and N is the number of samples during signal pulse time T.

8.3 SNR gain and Mean Error Analysis Simulations

Here a signal $s(t)$ is considered for SNR gain and mean error in parameter estimation under different SNR conditions (Monte Carlo simulation) as

$$s(t) = x_1(t) + x_2(t) + n(t), \tag{122}$$

where $n(t)$ is AWGN. $x_1(t)$ and $x_2(t)$ are quadratic chirp signals defined by

$$x_1(t) = \mathrm{e}^{i\pi 80t^3 + i\pi 40t^2 + i\pi 25t},\ x_2(t) = \mathrm{e}^{i\pi 60t^3 + i\pi 100t^2 + i\pi 21t}, \text{where } 0 \le t < 1\text{sec}. \tag{123}$$

8.3.1 SNR Gain Simulation

Monte Carlo simulation for 200 iterations has been performed to compare the SNR gain of ck-AGFS, ck-GTFT, time domain matched filtering, FrAF, and STFT for individual quadratic chirp components $x_1(t)$ and $x_2(t)$. The search range for the quadratic rate is considered to be (79: 0.1: 81) and (59 : 0.1: 61) for the first and second components, respectively. Similarly, the search range of the ck-AGFS angle is considered to be $(-88.1820° : 0.009° : -88.002°)$ and $(-85.329° : 0.009° : -85.149°)$ for the first and second component, respectively. Similarly, the search range of GTFT angle is considered $(-86.2759° : 0.009° : -86.0959°)$ and $(-80.6277° : 0.009° : -80.4477°)$ for first and second component respectively.Similarly, the search range of FrAF angle is considered $(-85.4543° : 0.09° : -83.6543°)$ and $(86.2376° : 0.09° : 88.0376°)$ for first and second component respectively.

As shown in the Fig. 7, time domain matched filtering gives the highest SNR in the case of AWGN, and it is equivalent to N_1, where N_1 is the product of the bandwidth and the pulse width. SNR gain of ck-STGTFT is observed to be lower than time domain matched filtering, close to the mathematically derived value ($\approx 0.57N_1$). We observe that ck-STGTFT also has a higher SNR gain compared to the ck-GTFT SNR gain ($\approx 0.5N_1$). STFT can not localise higher order chirp signals, so the SNR gain of STFT is found to be least among all, as shown in both graphs in Fig. 7 [49]. A nonlinear time-frequency distribution such as FrAF produces cross-terms during multicomponent signal analysis, so the SNR gain of FrAF is found to be less as compared to SNR gain of ck-GTFT, ck-AGFS in both graphs in Fig. 7. Hence, ck-AGFS SNR gain is higher than those of STFT, GTFT, and FrAF for multicomponent quadratic chirp signals.

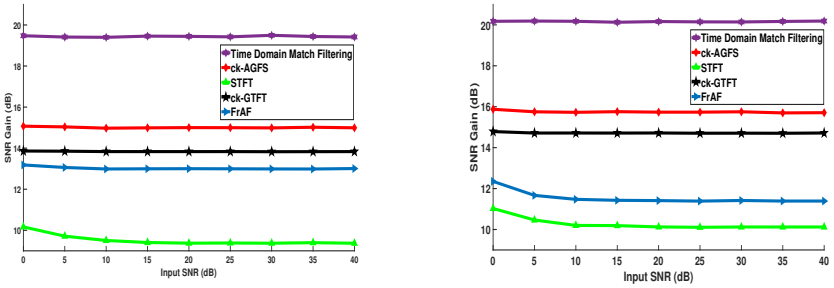

(a) (b)

Fig. 7 (a) SNR gain comparison of first component (b) SNR gain comparison of second component

8.3.2 Mean Error Analysis for Parameter Estimation

Monte Carlo simulation for 200 iterations has been performed to compare mean errors in estimating quadratic chirp parameters using ck-AGFS, ck-GTFT and FrAF of individual quadratic chirp components $x_1(t)$ and $x_2(t)$ of signal $s(t)$. The search range

of quadratic rate, ck-AGFS matched angle, and FrAF matched angle are considered similar to the search range for SNR gain analysis for the first and second components. The GTFT based parameter estimation algorithm is used as given in [37]. Fig. 8 shows the mean error in the estimation of first quadratic chirp component $x_1(t)$ parameters, in presence of second quadratic chirp component $x_2(t)$ and AWGN noise $n(t)$. Similarly, Fig. 9 shows the mean error in the estimation of second quadratic chirp component $x_2(t)$ parameters in presence of first quadratic chirp component $x_1(t)$ and AWGN noise $n(t)$. GTFT was calculated on the full signal length N, whereas ck-AGFS used an $N/2$ size sliding window over which the estimated parameters were averaged. FrAF produces cross-terms during multicomponent signal analysis, so it gives higher mean error as compared to GTFT and AGFS for estimating parameters of multicomponent chirp. As shown in Fig. 8 and Fig. 9, ck-AGFS based parameter estimation techniques give less mean error than ck-GTFT and FrAF based parameter estimation techniques for estimating parameters of multicomponent quadratic chirp.

Furthermore, the signal given by Eq. (97-98) is considered to analyse the effect of amplitude modulation in parameter estimation in the presence of noise. It is observed that parameter estimation fails below SNR of 0 dB, and the TFD spreads away from the true instantaneous frequency. Similar claims have also been reported in [54].

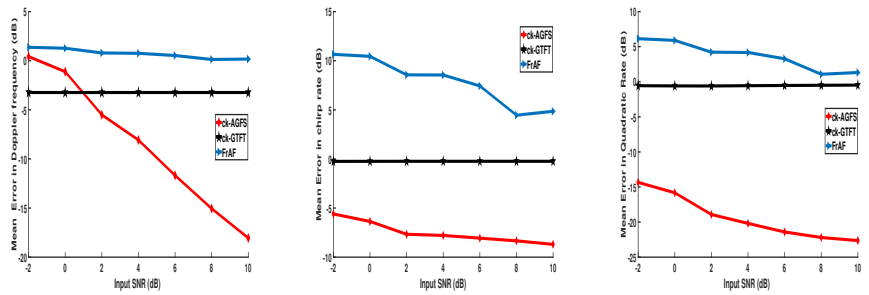

(a) (b) (c)

Fig. 8 Mean error comparisons for parameters of first component (a) Doppler frequency (b) chirp rate (c) quadratic rate

9 TFD of Long and Short Overlapping Chirps: Locally Optimised AGFS

The extraction method in section 7 works fine when multiple components of the signal have the same duration, and each component is present at each time instant. If one of the overlapping components is of shorter duration than the other, the optimal parameter search with a single fixed optimal sliding window gives unsatisfactory results in the regions where only one component is present. Similar to the adaptive fractional spectrogram (AFS), the above method also suffers from energy leakage if the signal is absent in certain regions [7, pp. 304]. This problem was noted, and a solution was proposed using locally optimised STFrFT [3, 4]. In a similar way, we use locally optimised AGFS to overcome these problems.

In the proposed approach, R numbers of AGFS spectrograms of the signal are constructed with a different choice of parameters (α, λ) and window variance (σ^2).

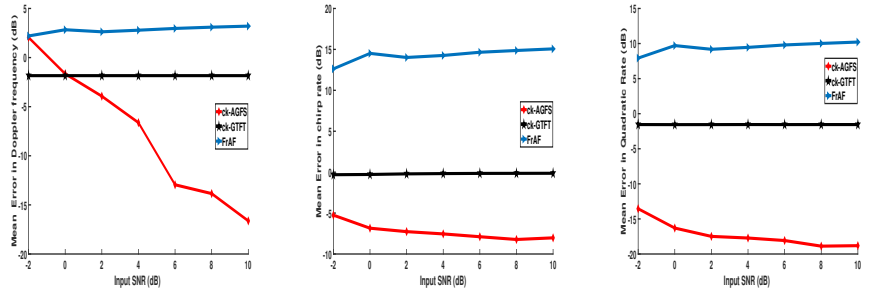

(a) (b) (c)

Fig. 9 Mean error comparisons for parameters of second component (a) Doppler frequency (b) chirp rate (c) quadratic rate

Let the spectrograms be labelled as $j = 0, 1, 2, ..., R-1$. All these R spectrograms are equally divided into P smaller blocks of the same dimension and let these small blocks in each spectrogram be labelled as $i = 0, 1, 2, ..., P-1$. The energy concentration measure (ECM) is calculated for each block of every spectrogram. Now, ECM of every i^{th} block of R spectrograms is compared, and least ECM valued block's i, and j value is stored, and these least ECM blocks are called optimum blocks. Finally, all optimum blocks are concatenated to make a P blocked locally optimised AGFS (LO-AGFS). In this approach, dividing R spectrograms plays a key role, and it mainly depends on the number and orientation of signal components in the time-frequency plane. LO-AGFS method gives the flexibility to analyse any frequency modulated signals by choosing optimum parameter (α, σ^2) and $h(\cdot)$ parameter of GTFT kernel in blocked locally optimised AGFS for constructing final AGFS. In the future, a robust way to divide LO-AGFS can be explored.

Here four nearby amplitude quadratic chirp components that are present in different but partially overlapping regions along time are considered. Parameters of different components and mathematical equation of the combined signal are mentioned in Table 9 and Eq.(125) respectively.

$$x_1(t) = \begin{cases} e^{i\pi c_1 t^3 + i\pi a_1 t^2 + 2i\pi f_{d1}} & 0 \le t < 0.5\text{sec} \\ e^{i\pi c_2 t^3 + i\pi a_2 t^2 + 2i\pi f_{d2}} & 0.5 \le t < 0.75\text{sec} \end{cases},$$
$$x_2(t) = \begin{cases} e^{i\pi c_3 t^3 + i\pi a_3 t^2 + 2i\pi f_{d3}} & 0.5 \le t < 1\text{sec} \\ e^{i\pi c_4 t^3 + i\pi a_4 t^2 + 2i\pi f_{d4}} & 0 \le t < 1\text{sec} \end{cases}, \tag{124}$$

$$x(t) = 1.5e^{-0.08t} \cdot x_1(t) + 2e^{-0.04t} \cdot x_2(t). \tag{125}$$

Fig. 10 (a-b) shows the locally optimised ck-AGFS and locally optimised STFrFT based spectrogram (considering $\lambda = 0$ or $h(\cdot) = 0$ in GTFT kernel) respectively, obtained as per the above method.Fig. 10 (c-d) the time slices of these at 0.61 seconds, and these indicate that locally optimised ck-AGFS can separate the components more distinctly as compared to locally optimised STFrFT based spectrogram, due to the presence of the cubic phase term in the kernel of ck-GTFT.

Table 9 Simulation parameters of four amplitude modulated closely space long and short quadratic chirps

multicomponent long and short chirps parameter						
$\tau\ (s)$	$f_s\ (Hz)$	$c_1\ (Hz^3)$	$c_2\ (Hz^3)$	$c_3\ (Hz^3)$	$c_4\ (Hz^3)$	$a_1\ (Hz^2)$
1	600	140	130	100	80	30
$a_2\ (Hz^2)$	$a_3\ (Hz^2)$	$a_4\ (Hz^2)$	$f_{d1}\ (Hz)$	$f_{d2}\ (Hz)$	$f_{d3}\ (Hz)$	$f_{d4}\ (Hz)$
40	50	60	90	70	66	60

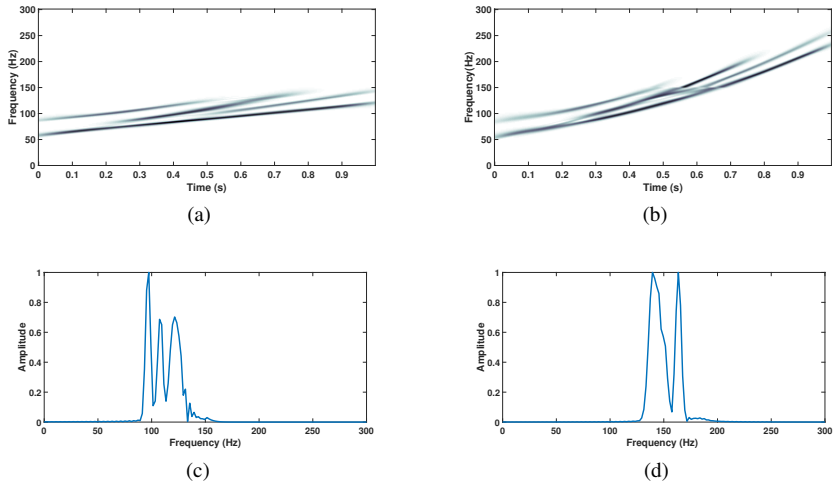

Fig. 10 Spectrogram view of closely spaced multicomponent long and short chirps (a) Locally optimised ck-AGFS (b) Locally optimised STFrFT based spectrogram (c) Time slice of locally optimised ck-AGFS at 0.61 sec. (d) Time slice of locally optimised STFrFT based spectrogram at 0.61 seconds

10 Real Multicomponent Bat Echolocation Signal Analysis

A real multicomponent bat echolocation signal is analysed using locally optimised ck-AGFS to demonstrate the effectiveness of AGFS. As shown in Fig. 11(a-e), TFDs such as STFT, WVD, EMBD, CKD, and AFS are unable to provide a high concentration TFD of the signal. Similar to [11, 34], four components of the signal are detected with LO-ck-AGFS. Multiple locally optimised ck-AGFS blocks with locally optimum α,λ, and window variance are concatenated to make final LO-ck-AGFS and detailed method described in section 9. LO-ck-AGFS of bat signal is shown in Fig. 11(f). From the figure, it can be inferred that LO-ck-AGFS is comparatively better than other TFDs to represent multicomponent bat signal.

11 AGFS Application: AGFS of SAR data

SAR is an imaging radar, which provides high resolution two-dimensional images from the reflectivity of a scene. In conventional SAR signal processing algorithms

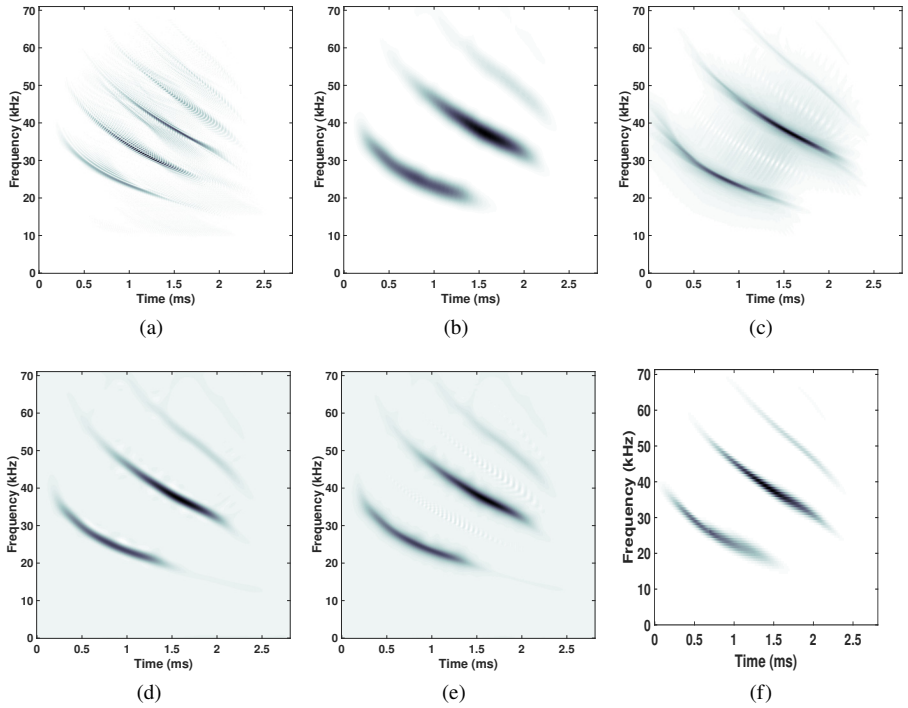

Fig. 11 Spectrogram view of real bat echolocation signal using different TFDs (a) WVD (b) STFT (c) AFS (d) CKD (e) EMBD (f) LO-ck-AGFS

like range-Doppler algorithm (RDA), 2D matched filtering is performed for focusing SAR image in range and azimuth directions. Range cell migration compensation is performed after range compression to avoid range cell migration over SAR integration time. In the case of stationary targets, SAR forms a linear chirp in the azimuth direction due to constant azimuth velocity motion of SAR carrying flight [16]. But in the case of ground moving targets, SAR forms a quadratic chirp in azimuth direction [20, 29, 52, 53]. The ck-AGFS can be used for the representation of these multicomponent quadratic chirps.

11.1 Comparison of Spectrograms of Simulated SAR Data

SAR data in azimuth direction is represented in the TF plane after range compression and range cell migration compensation. SAR data of 1 *m* resolution cell has been simulated to demonstrate the advantages of using ck-AGFS over conventional STFT based spectrogram. Two nearby ground moving point targets are simulated, which have the same position along range direction but different positions in the azimuth direction. Hence their impulse response in range direction overlap. Both ground moving target has the same centre slant range of 2000 cells, SNR of -10dB, tangential

velocity of 10 m/s, radial velocity of 20 m/s, a tangential acceleration of 10 m/s^2, and a zero radial acceleration, but are separated in azimuth by 130 azimuth cells. For the simulation, SAR transmitting frequency of 1 GHz, radar waveform bandwidth of 160 MHz, and a SAR platform velocity of 200 m/s was considered.

As shown in Fig. 12(a), the STFT based spectrogram at its optimum window, is unable to resolve two nearby ground moving targets. Whereas, as shown in Fig. 12(b), ck-AGFS at its optimum window, and matched ck-STGTFT can represent each ground moving target separately. Finally, Fig. 12(c) shows the focused SAR image of two ground moving point targets after phase correction.

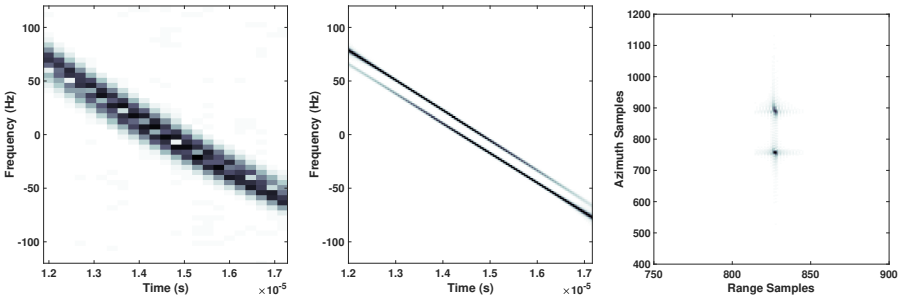

(a) (b) (c)

Fig. 12 Comparison of spectrogram for simulated ground moving point targets of SAR (a) STFT based spectrogram (b) ck-AGFS (c) Focused SAR image

12 Conclusion

In this paper, novel AGFS based on STGTFT is proposed, which can provide a high concentration, high resolution, cross-term free TFD. This is illustrated by considering two nearby amplitude-modulated quadratic chirps whose parameters change in between signal duration. Matched ck-AGFS at optimum window length resolves the components more precisely than STFT and other TFDs. The optimum window length of ck-AGFS can be easily estimated from the signal length at matched ck-STGTFT of ck-AGFS. The uncertainty principle is derived for STGTFT, FrAF, and FrWVD, and TBP of STGTFT for quadratic chirp is shown to be less than the TBP of STFrFT, STFT, and lower bound of TBP of FrAF. The extraction algorithm is demonstrated for signals having two nearby amplitude-modulated quadratic chirps whose parameters change during the length, and they indicate better performance of ck-AGFS as compared to the STFT based spectrogram. AGFS can be used to analyse a large variety of multicomponent frequency modulated signals by choosing the appropriate $h(\cdot)$ parameter in GTFT kernel. A mathematical derivation of the SNR gain of ck-AGFS for analysing multicomponent quadratic chirps shows that it is higher than those of GTFT, FrAF, and STFT, and the same was corroborated in simulations. ck-AGFS based parameter estimation is demonstrated to be better than GTFT and FrAF based parameter estimation by reporting mean errors in parameter estimation.

The superiority of LO-ck-AGFS is demonstrated as compared to locally optimised STFrFT based spectrogram for the representation of closely spaced long and short overlapping chirps. LO-ck-AGFS outperformed other well-known TFDs in representing a real multicomponent bat signal. Local optimum window and global optimum window-based STGTFT follows the property of index additivity of angle (similar to FrFT); hence, AGFS is computationally efficient. An application of AGFS to estimate higher polynomial phase components in SAR ground moving target imaging is presented, and it can be applied to similar applications, such as radar, sonar, and biomedical signal processing for representation, extraction, and parameter estimation of multicomponent frequency modulated signals. In the future, the application of AGFS for SAR ground moving target detection and imaging will be explored further and compared with existing methods. AGFS can be used for the representation of a different variety of signals by appropriate selection of the parametric function $h(\cdot)$ in the GTFT kernel.

Acknowledgements The authors would like to thank the DRDO, Ministry of Defence, Govt. of India for sponsorship of Peeyush Sahay, Sc 'E' (Ph.D. student), and B. S. Teza, Sc 'C' (Master student) under the R&D scheme, at IIT Bombay. The authors would like to thank Mr. Shubham Anand Jain (B.Tech, IIT Bombay), Mr. Ameya Anjarlekar (B.Tech, IIT Bombay), Mr. Adway Girish (B.Tech, IIT Bombay), Mr. Shubham Kar (B.Tech, IIT Bombay), Mr. Ayush Agarwal (B.Tech, IIT Dharwad), Mr. Shaan Ul Haque (B.Tech, IIT Bombay), Mr. Izaz Ahamed Shaik Rasheed (M.Tech, IIT Bombay), and Mr. Gaurav Pooniwala (B.Tech, IIT Bombay) for improving the quality of the paper. The authors wish to thank Curtis Condon, Ken White, and Al Feng of the Beckman Institute of the University of Illinois for the bat data and for permission to use it in this paper.

References

1. Almeida, L.B.: The fractional Fourier transform and time-frequency representations. IEEE Transactions on signal processing **42**(11), 3084–3091 (1994)
2. Auger, F., Flandrin, P., Lin, Y.T., McLaughlin, S., Meignen, S., Oberlin, T., Wu, H.T.: Time-frequency reassignment and synchrosqueezing: An overview. IEEE Signal Processing Magazine **30**(6), 32–41 (2013)
3. Awal, M.: Design and optimisation of time-frequency analysis for multichannel neonatal eeg background features in term neonates with hypoxic ischaemic encephalopathy: characterisation, classification and neurodevelopmental outcome prediction. Ph.D. thesis, University of Queensland, Brisbane, Australia (2018)
4. Awal, M.A., Ouelha, S., Dong, S., Boashash, B.: A robust high-resolution time–frequency representation based on the local optimization of the short-time fractional Fourier transform. Digital Signal Processing **70**, 125–144 (2017)
5. Bai, X., Tao, R., Liu, L.J., Zhao, J.: Autofocusing of SAR images using STFRFT-based preprocessing. Electronics Letters **48**(25), 1622–1624 (2012)
6. Barkat, B., Abed-Meraim, K.: Algorithms for blind components separation and extraction from the time-frequency distribution of their mixture. EURASIP Journal on Advances in Signal Processing **2004**(13), 2025–2033 (2004)
7. Boashash, B.: Time-Frequency Signal Analysis and Processing: a comprehensive reference. Academic Press, Orlando, FL, USA (2015)

8. Boashash, B., Khan, N.A., Ben-Jabeur, T.: Time-frequency features for pattern recognition using high-resolution TFDs: A tutorial review. Digital Signal Processing **40**, 1–30 (2015)
9. Boashash, B., Ouelha, S.: Designing high-resolution time–frequency and time–scale distributions for the analysis and classification of non-stationary signals: a tutorial review with a comparison of features performance. Digital Signal Processing **77**, 120–152 (2018)
10. Capus, C., Brown, K.: Fractional Fourier transform of the gaussian and fractional domain signal support. IEE Proceedings-Vision, Image and Signal Processing **150**(2), 99–106 (2003)
11. Capus, C., Brown, K.: Short-time fractional Fourier methods for the time-frequency representation of chirp signals. The Journal of the Acoustical Society of America **113**(6), 3253–3263 (2003)
12. Che Tian-Wen, and Li Bing-Zhao, and Xu Tian-Zhou: The ambiguity function associated with the linear canonical transform. EURASIP Journal on Advances in Signal Processing **2012**(1), 1–14 (2012)
13. Chen, V.C.: The Micro-Doppler effect in Radar. Artech House, Norwood, MA (2019)
14. Chen, V.C., Tahmoush, D., Miceli, W.J.: Radar Micro-Doppler Signatures: Processing and Applications. Institution of Engineering and Technology, Herts, UK (2014)
15. Cohen, L.: Time-frequency analysis: theory and applications. Prentice hall, Englewood Cliffs, NJ (1995)
16. Cumming, I.G., Wong, F.H.: Digital processing of Synthetic Aperture Radar data. Artech house, Norwood, MA (2005)
17. Djurović, I., Ioana, C., Thayaparan, T., Stanković, L., Wang, P., Popović, V., Simeunović, M.: Cubic-phase function evaluation for multicomponent signals with application to SAR imaging. IET Signal Processing **4**(4), 371–381 (2010)
18. Djurovic, I., Thayaparan, T., Stankovic, L.: SAR imaging of moving targets using polynomial Fourier transform. IET Signal Processing **2**(3), 237–246 (2008)
19. El-Mashed, M., Zahran, O., Dessouky, M.I., El-Kordy, M., El-Samie, F.A.: Synthetic aperture radar imaging with fractional Fourier transform and channel equalization. Digital Signal Processing **23**(1), 151–175 (2013)
20. Huang, P., Liao, G., Yang, Z., Xia, X.G., Ma, J., Zheng, J.: Ground maneuvering target imaging and high-order motion parameter estimation based on second-order keystone and generalized Hough-HAF transform. IEEE Transactions on Geoscience and Remote Sensing **55**(1), 320–335 (2017)
21. Iatsenko, D., McClintock, P.V., Stefanovska, A.: Linear and synchrosqueezed time–frequency representations revisited: Overview, standards of use, resolution, reconstruction, concentration, and algorithms. Digital Signal Processing **42**, 1–26 (2015)
22. Khan, N.A., Boashash, B.: Instantaneous frequency estimation of multicomponent nonstationary signals using multiview time-frequency distributions based on the adaptive fractional spectrogram. IEEE Signal Processing Letters **20**(2), 157–160 (2013)

23. Li, X., Bi, G., Ju, Y.: Quantitative SNR analysis for ISAR imaging using LPFT. IEEE Transactions on Aerospace and Electronic Systems **45**(3), 1241–1248 (2009)
24. Liu, J.G., Yuan, B.C.: The analysis and simulation of the detectors based on FRFT statistic performance. In: 2008 Asia Simulation Conference-7th International Conference on System Simulation and Scientific Computing, pp. 1543–1548 (2008)
25. Ozaktas, H.M., Arikan, O., Kutay, M.A., Bozdagt, G.: Digital computation of the fractional Fourier transform. IEEE Transactions on signal processing **44**(9), 2141–2150 (1996)
26. Pei, S.C., Huang, S.G.: STFT with adaptive window width based on the chirp rate. IEEE Transactions on Signal Processing **60**(8), 4065–4080 (2012)
27. Pelich, R., Longépé, N., Mercier, G., Hajduch, G., Garello, R.: Vessel refocusing and velocity estimation on SAR imagery using the fractional Fourier transform. IEEE Transactions on Geoscience and Remote Sensing **54**(3), 1670–1684 (2016)
28. Peng, B., Wei, X., Deng, B., Chen, H., Liu, Z., Li, X.: A sinusoidal frequency modulation Fourier transform for radar-based vehicle vibration estimation. IEEE Transactions on Instrumentation and Measurement **63**(9), 2188–2199 (2014)
29. Perry, R., Dipietro, R., Fante, R.: SAR imaging of moving targets. IEEE Transactions on Aerospace and Electronic Systems **35**(1), 188–200 (1999)
30. Pooniwala, G.: The generalised time frequency transform: Properties and application. B.tech. thesis, Indian Institute of Technology, Bombay, Mumbai, India (2014)
31. Popović, V., Djurović, I., Stanković, L., Thayaparan, T., Daković, M.: Autofocusing of SAR images based on parameters estimated from the PHAF. Signal Processing **90**(5), 1382–1391 (2010)
32. Rui-Feng Bai, B.Z.L., Cheng, Q.Y.: Wigner-Ville distribution associated with the linear canonical transform. Journal of Applied Mathematics pp. 1–14 (2012)
33. Sahay, P., Anjarlekar, A., Jain, S.A., , Radhakrishna, P., Gadre, V.M.: Generalized fractional matched filtering and its applications. In: Twenty Sixth National Conference on Communications (NCC), (in press) (2020)
34. Sahay, P., Shaik Rasheed, I.A., Jain, S.A., Anjarlekar, A., Radhakrishna, P., Gadre, V.M.: Generalized fractional ambiguity function and its applications. Circuits, Systems, and Signal Processing, (in press) (2020). DOI 10.1007/s00034-020-01398-7
35. Sahay, S., Pande, D., Wing, N., Gadre, V., Sohani, P.: A novel generalized time-frequency transform inspired by the fractional Fourier transform for higher order chirps. In: International Conference on Signal Processing and Communications (SPCOM), pp. 1–5 (2012)
36. Sahay, S.B.: Parameter estimation of chirp signals. Ph.D. thesis, Indian Institute of Technology, Bombay, Mumbai, India (2015)
37. Sahay, S.B., Meghasyam, T., Roy, R.K., Pooniwala, G., Chilamkurthy, S., Gadre, V.: Parameter estimation of linear and quadratic chirps by employing the fractional fourier transform and a generalized time frequency transform. Sadhana **40**(4), 1049–1075 (2015)

38. Sejdić, E., Djurović, I., Jiang, J.: Time–frequency feature representation using energy concentration: An overview of recent advances. Digital Signal Processing **19**(1), 153–183 (2009)
39. Sejdić, E., Djurović, I., Stanković, L.: Fractional Fourier transform as a signal processing tool: An overview of recent developments. Signal Processing **91**(6), 1351–1369 (2011)
40. Shinde, S., Gadre, V.M.: An uncertainty principle for real signals in the fractional Fourier transform domain. IEEE Transactions on Signal Processing **49**(11), 2545–2548 (2001)
41. Song, Y.E., Zhang, X.Y., Shang, C.H., Bu, H.X., Wang, X.Y.: The Wigner-Ville distribution based on the linear canonical transform and its applications for QFM signal parameters estimation. Journal of Applied Mathematics pp. 1–8 (2014)
42. Stankovic, L., Dakovic, M., Thayaparan, T.: Time-Frequency Signal Analysis with Applications. Artech house, Norwood, MA, USA (2014)
43. Starosielec, S., Hägele, D.: Discrete-time windows with minimal rms bandwidth for given rms temporal width. Signal Processing **102**, 240–246 (2014)
44. Tao, R., Deng, B., Zhang, W.Q., Wang, Y.: Sampling and sampling rate conversion of band limited signals in the fractional Fourier transform domain. IEEE Transactions on Signal Processing **56**(1), 158–171 (2008)
45. Tao, R., Li, X.M., Li, Y.L., Wang, Y.: Time-delay estimation of chirp signals in the fractional Fourier domain. IEEE Transactions on Signal Processing **57**(7), 2852–2855 (2009)
46. Tao, R., Li, Y.L., Wang, Y.: Short-time fractional Fourier transform and its applications. IEEE Transactions on Signal Processing **58**(5), 2568–2580 (2010)
47. Tao, R., Song, Y.E., Wang, Z.J., Wang, Y.: Ambiguity function based on the linear canonical transform. IET Signal Processing **6**(6), 568–576 (2012)
48. Thayaparan, T., Stankovic, L., Wernik, C., Dakovic, M.: Real-time motion compensation, image formation and image enhancement of moving targets in ISAR and SAR using S-method-based approach. IET Signal Processing **2**(3), 247–264 (2008)
49. Xia, X.G., Wang, G., Chen, V.C.: Quantitative snr analysis for ISAR imaging using joint time-frequency analysis-short time Fourier transform. IEEE Transactions on Aerospace and Electronic systems **38**(2), 649–659 (2002)
50. Xinghao, Z., Ran, T., Bing, D.: Practical normalization methods in the digital computation of the fractional Fourier transform. In: Proceedings of 7th International Conference on Signal Processing, pp. 105–108 (2004)
51. Xu, M., Tang, W.: Multi-component LFM signal filtering based on the short-time fractional Fourier transform. In: Proceedings of the 32nd Chinese Control Conference, pp. 4507–4512 (2013)
52. Yang, J., Liu, C., Wang, Y.: Detection and imaging of ground moving targets with real SAR data. IEEE Transactions on Geoscience and Remote Sensing **53**(2), 920–932 (2015)
53. Yang, J., Zhang, Y.: An airborne SAR moving target imaging and motion parameters estimation algorithm with azimuth-dechirping and the second-order keystone transform applied. IEEE Journal of Selected Topics in Applied Earth Observations and Remote Sensing **8**(8), 3967–3976 (2015)

54. Yang, Y., Peng, Z., Dong, X., Zhang, W., Meng, G.: Application of parameterized time-frequency analysis on multicomponent frequency modulated signals. IEEE Transactions on Instrumentation and Measurement **63**(12), 3169–3180 (2014)
55. Yang, Y., Peng, Z., Dong, X., Zhang, W., Meng, G.: General parameterized time-frequency transform. IEEE Transactions on Signal Processing **62**(11), 2751–2764 (2014)
56. Yang, Y., Zhang, W., Peng, Z., Meng, G.: Multicomponent signal analysis based on polynomial chirplet transform. IEEE Transactions on Industrial Electronics **60**(9), 3948–3956 (2013)
57. Zayed, A.I.: A convolution and product theorem for the fractional Fourier transform. IEEE Signal processing letters **5**(4), 101–103 (1998)
58. Zhu, J.d., Li, J.l., Gao, X.d., Ye, L.B., Dai, H.y.: Adaptive threshold detection and estimation of linear frequency-modulated continuous-wave signals based on periodic fractional Fourier transform. Circuits, Systems, and Signal Processing **35**(7), 2502–2517 (2016)
59. Zuo, L., Li, M., Liu, Z., Ma, L.: A high-resolution time-frequency rate representation and the cross-term suppression. IEEE Transactions on Signal Processing **64**(10), 2463–2474 (2016)